Mon. Not. R. Astron. Soc. **000**, 000–000 (0000) Printed 1 February 2008 (MN LATEX style file v2.2)

Radiative Torque Alignment: Essential Physical Processes

Thiem Hoang [1⋆], and A. Lazarian [2†]
Department of Astronomy, University of Wisconsin, Madison, WI 53706, USA

1 February 2008

arXiv:0707.3645v2 [astro-ph] 22 Oct 2007

ABSTRACT

We study the physical processes that affect the alignment of grains subject to radiative torques (RATs). To describe the action of RATs, we use the analytical model (AMO) of RATs introduced in Paper I. We focus our discussion on the alignment by anisotropic radiation flux with respect to magnetic field, which defines the axis of grain Larmor precession. Such an alignment does not invoke paramagnetic dissipation (i.e. Davis-Greenstein mechanism), but, nevertheless, grains tend to be aligned with long axes perpendicular to the magnetic field. When we account for thermal fluctuations within grain material, we show that for grains, which are characterized by a triaxial ellipsoid of inertia, the zero-J attractor point obtained in our earlier study develops into a low-J attractor point. The value of angular momentum at the low-J attractor point is the order of the thermal angular momentum corresponding to the grain temperature. We show that, for situations when the direction of radiative flux was nearly perpendicular to a magnetic field, the alignment of grains with long axes parallel to the magnetic field (i.e. "wrong alignment") reported in Paper I, disappears in the presence of thermal fluctuations. Thus, all grains are aligned with their long axes perpendicular to the magnetic field. To gain insight into the origin and stability of the low-J attractor points, we study the dynamics of the crossovers in the presence of both RATs and thermal fluctuations. We study effects of stochastic gaseous bombardment and show that gaseous bombardment can drive grains from low-J to high-J attractor points in cases when the high-J attractor points are present. As the alignment of grain axes with respect to angular momentum is higher for higher values of J, counter-intuitively, gaseous bombardment can increase the degree of grain alignment in respect to the magnetic field. We also study the effects of torques induced by H_2 formation and show that they can change the value of angular momentum at high-J attractor point, but marginally affect the value of angular momentum at low-J attractor points. We compare the AMO results with those obtained using the direct numerical calculations of RATs acting upon irregular grains and validate the use of the AMO for realistic situations of RAT alignment.

Key words: ISM- Magnetic field- polarization, ISM: dust-extinction

1 INTRODUCTION

Polarization from absorption and emission by aligned grains is widely believed to trace magnetic field topology (see Hildebrand et al. 2000, Hildebrand 2002; Aitken et al. 2002; Hough et al. 1989). The reliability of the interpretation of polarization maps in terms of magnetic fields depends crucially on the understanding of grain alignment theory.

When, nearly 60 years ago, the polarization of starlight was discovered (Hall 1949; Hilner 1949), it was immediately explained by absorption by elongated dust grains, which are aligned with respect to the interstellar magnetic field. Since then, the problem of grain alignment has been addressed by many authors (see a recent review by Lazarian 2007 and references therein). As a result, substantial progress has been made towards understanding how these tiny particles can become aligned.

The original theory of grain alignment formulated by Davis & Greenstein (1951) is based on the paramagnetic dissipation of energy for a grain rotating in an *external* magnetic field. However, the paramagnetic relaxation time-scale for a typical interstellar field strength is long compared to the gas damping time. Moreover, this mechanism has been found to be more efficient for small grains (see Lazarian 1997a; Roberge & Lazarian 1999), contrasting with obser-

⋆ E-mail: hoang@astro.wisc.edu
† E-mail:lazarian@astro.wisc.edu

© 0000 RAS

vation data, which have testified that small grains are not aligned (Kim & Martin 1995; Andersson & Potter 2007).

Study of the paramagnetic alignment mechanism was given new life by Purcell (1979). In his classical paper, Purcell suggested three processes that can spin a grain up to suprathermal rates (i.e., much higher than thermal value): H_2 formation, photoemission, and the variation of the accommodation coefficient over the grain surface. H_2 formation was identified as the most powerful of these three processes. In terms of alignment, fast rotation is advantageous, as fast rotating grains are immune to randomization by gas bombardment. As a result, paramagnetic dissipation can give rise to good alignment of angular momentum with the magnetic field. An obvious limitation of the Purcell mechanism is that the spin-up process is most efficient, provided that a sufficient fraction of hydrogen is in atomic form. Therefore, this mechanism would fail in dark molecular clouds where most of the hydrogen is in molecular form. In fact, all spin-up processes fail in molecular clouds (see Lazarian, Goodman & Myers 1997; Roberge & Lazarian 1999), while observations have testified that the grains were aligned there (see Ward-Thompson et al. 2000).

Nevertheless, combining the ideas of suprathermal rotation with magnetic inclusions, in the spirit of the classical Jones & Spitzer (1967) paper, researchers hoped to explain the observational data. For instance, a model by Mathis (1986) provided a good fit to the observed Serkowski polarization curve (Serkowski 1975). Problems concerning the Purcell (1979) alignment mechanism became obvious, however, when Lazarian & Draine (1999a) reported the effect of thermal trapping. This effect stems from the coupling of vibrational and rotational degrees of freedom via the internal relaxation (e.g. Barnett relaxation; Purcell 1979). Thermally trapped grains undergo fast flips that average out un-compensated Purcell torques. Later, Lazarian & Draine (1999b) reported a new effect which they termed nuclear relaxation[1]; they showed this to be 10^6 times stronger than the Barnett relaxation. After this, it became clear that most of the interstellar grains cannot be spun up by Purcell torques.

The mechanical alignment mechanism, which is based on the relative motion of gas and dust, was pioneered by Gold (1952a). However, this mechanism, as well as its more sophisticated cousins (Lazarian 1995, 1997; Lazarian & Efroimsky 1996; Lazarian, Efroimsky & Ozik 1996), requires supersonic motion of gas relative to dust (see Purcell 1969; Lazarian 1994; Roberge, Hanany & Messinger 1995; Lazarian 1997b), and this is only available in special circumstances. In his original paper, Gold (1952b) proposed collisions between clouds as a way to drive supersonic motion. Soon after this, Davis (1955) pointed out that such a process can only align grains in a tiny fraction of the interstellar medium (ISM). Other, more promising means of obtaining supersonic drift are ambipolar diffusion (Roberge & Hanany 1990, Roberge, Hanany & Messinger 1995) and MHD turbulence (Lazarian 1994; Lazarian & Yan 2002; Yan & Lazarian 2003; Yan, Lazarian & Draine 2004). Nevertheless, while applicable for particular environments, the mechanical mechanisms are unable to explain the ubiquitous alignment of dust in a diffuse medium and molecular clouds. A more promising mechanism is the mechanical alignment of helical grains, first mentioned in Lazarian (1995) and Lazarian, Goodman & Myers (1997). We briefly described this in Lazarian (2007) and Lazarian & Hoang (2007a). The consequences of this have to be evaluated, but these are beyond the scope of the present paper.

Alignment by radiative torques (RATs) has recently become a favored mechanism to explain grain alignment. This mechanism was initially proposed by Dolginov & Mytraphanov (1976), but was not sufficiently appreciated at the time of its introduction. Draine & Weingartner (1996, 1997, hereafter DW96 and DW97) reinvigorated the study of the RAT mechanism by showing that RATs induced by anisotropic radiation upon rather arbitrarily shaped grains can spin-up and directly align them with the magnetic field. These papers refocused attention on the RAT mechanism and made it a promising candidate to change the grain alignment paradigm. It is also very noble that Bruce Draine has kindly modified the publicly available DDSCAT code (Draine & Flatau 1994) to include RATs. This has enabled other researchers to access a useful tool for studying the RAT alignment.

The RAT mechanism seems to be able to address major puzzles presented by observations. For instance, the observation of polarized emission emanating from starless cores (see Ward-Thompson 2000, 2002) initially seemed completely unexplainable.[2] Indeed, all mechanisms seemed to fail in such cores, which are presumably close to thermodynamic equilibrium (see Lazarian, Goodman & Myers 1997). The RATs seem to be too weak as well (DW96). However, Cho & Lazarian (2005, hereafter CL05) found that the efficiency of RATs increases fast with grain size (see also Lazarian & Hoang 2007a), and thus large grains can still be aligned in dark clouds. They found that grains as large as $0.6\mu m$ can be aligned in dark clouds by radiation attenuated by the column density with $A_V \approx 10$. This was for much higher extinction than expected in the absence of embedded stars (see DW96), and was claimed to be observed with optical and near infrared polarimetry (Acre et al. 1998).

The pre-stellar cores studied in Ward-Thompson et al. (2000) correspond to $A_V = 50 - 60$; the shielding column, assuming uniformity, is approximately half of these values. However, Crutcher et al. (2004) pointed out that polarization data do not sample the innermost core regions[3], and this provides an explanation for polarization "holes" (see Matthews & Wilson 2000, 2002; Matthews et al. 2001; Lai et al. 2002). The reported decrease in the percentage polarization with the optical depth also agrees well with the findings in CL05.

The approach of CL05 was further elaborated in the studies by Pelkonen et al (2007) and Bethell et al. (2007), in which the synthetic maps obtained via MHD simulations

[1] The Barnett relaxation arises from the unpaired electron spins in the grain. The nuclear relaxation is resulted from unpaired nuclear spins. The mechanisms are different and should not be mixed up.

[2] These findings are also contrasting with observational claims based on visible and near-infrared radiation (Goodman et al. 1995). The difference in results was explained in Lazarian (2003)

[3] The peaks A_V of 150 were claimed for the clouds in Pagani et al. (2004). According to Crutcher (2007, private communication) these peaks are likely not to produce polarized dust emission.

were analyzed. In particular, Bethell et al. (2007) obtained the polarization maps were for a simulated cloud with peaks of extinction A_V as high as 25. The study showed non-trivial nature of radiative transfer in a fractal turbulent cloud, and confirmed the the ability of aligned grains to trace a magnetic field in dark clouds and proved a decrease of percentage polarization at the highest A_V. Note that the studies above were in contrast to the previous studies, which used rather arbitrary criteria (e.g. $A_V = 3$) for the alignment to shut down, or even more unrealistic assumption that all grains were perfectly aligned.

Similarly, the change of the degree of polarization with optical depth observed by Whittet et al. (2001) was also explained by RATs in Lazarian (2003, 2007). Detailed modeling of this effect is provided in Whittet et al. (2007) and Hoang & Lazarian (in preparation).

The encouraging correspondence of the theoretical expectations[4] and the observed polarization arising from aligned grains makes it essential to understand the reason why RATs align grains. In our first paper (Lazarian & Hoang 2007a, hereafter Paper I), we subjected to scrutiny the properties of RATs. Using a simple analytical model (AMO) of a helical grain we studied the properties of RATs and the alignment driven by such RATs. The analytical results were found to be in good correspondence with numerical calculations for irregular grains obtained with DDSCAT. Evoking the generic properties of the RAT components, we explained the RAT alignment of grains in both the absence and presence of magnetic fields. Intentionally, for the sake of simplicity, in Paper I we studied a simplified dynamical model to demonstrate the effect of the RAT alignment. This model disregards the wobbling of grain axes with respect to the angular momentum that arises from thermal fluctuations (Lazarian 1994; Lazarian & Roberge 1997), and thermal flipping of grains (Lazarian & Draine 1999a, b). The simplifications allowed us to provide a vivid illustration of the RAT alignment, however, there is still a question concerning the modification of the alignment by thermal fluctuations, as well as the action of additional (e.g. random) torques.

The first study to combine the RAT alignment and the physics of thermal fluctuations and flipping was carried out by Weingartner & Draine (2003; hereafter WD03). They studied the alignment by RATs produced by a monochromatic radiation field and for one particular radiation direction $\psi = 70^\circ$, taking into account thermal fluctuations and thermal flipping. They observed the appearance of new attractor points at low angular momentum, but the underlying physics of this effect remained unclear.

WD03 also posed a question concerning what is happening when the entire spectrum of the interstellar radiation field (the ISRF) is accounted for, and when radiation arrives from other directions. Their study does not consider the effect of gaseous bombardment and effects of H_2 formation. We address these and other issues in the present below.

[4] Although being a step forward compared to the earlier naive predictions of polarization which were mostly detached from the grain alignment theory, CL05 and the follow up studies (e.g. Pelkonen et al. 2007; Bethell et al. 2007; Cho & Lazarian 2007) are also not exact, as they are based on the alignment efficiencies inferred from idealized numerical studies, rather than on the exact RAT alignment theory.

The structure of the paper is as follows. In §2 we present current theoretical understandings of the RAT alignment and formulate our theoretical predictions. We briefly describe thermal wobbling and our method of averaging RATs in § 3. In §4 we derive the analytical expressions for RATs for the AMO averaged over thermal fluctuations, and study the influence of thermal fluctuations to the grain alignment by RATs. In §5 we study the alignment for irregular grains with RATs from DDSCAT. We provide an explanation to the appearance of the low attractor point based on the AMO and discuss the stability of low and high J attractor points in §6. We study the physics of crossovers induced by RATs in §7. We consider fast alignment in the presence of thermal fluctuations in §8. In §9 and §10 show the influences of random collisions and H_2 formation torques in the framework of RAT alignment for both the AMO and irregular grains. An extended discussion is presented in §11. Finally, we summarize our results in §12.

2 THEORETICAL CONSIDERATIONS

In Paper I we provided analytical calculations for RATs for a grain model that consists of a perfectly reflecting oblate spheroid with a "massless" mirror attached at its pole (see the upper panel in Fig. 1). This helical grain demonstrates RATs that are similar to those of irregular grains obtained by DDSCAT (see Paper I).

The basic properties of RATs were the subject of a detailed analysis in Paper I. We established that the projection of RATs onto $\hat{\mathbf{e}}_3$ axis (i.e. Q_{e3}; see the upper panel in Fig. 1) determines the precession of the grain axis about the radiation direction. This component is also present for non-helical (e.g. simple spheroid) grains, and neither case induces grain alignment. It is the other two RAT components, Q_{e1} and Q_{e2}, that are responsible for grain alignment. In Paper I we explain why the RAT alignment tends to occur with the long axis of the grain either perpendicular to the magnetic field or perpendicular to the radiation direction (the choice of which, for a given external magnetic field, is determined by the ratio of the rate of radiative precession about the radiation direction and Larmor precession).

In Paper I we found an important parameter that affects the grain alignment, the ratio $Q_{e1}^{max}/Q_{e2}^{max}$, where Q_{e1}^{max} and Q_{e2}^{max} are amplitudes of Q_{e1} and Q_{e2}, respectively. Different grain shapes illuminated by different radiation fields can have different ratios $Q_{e1}^{max}/Q_{e2}^{max}$, and thus the resulting alignment is different.

We carried out the study of the RAT alignment in Paper I assuming that the grain always rotates about its principal inertia axis $\mathbf{a}_1$, corresponding to the maximal moment of inertia (hereafter called the maximal inertia axis). However, this assumption is only valid for fast rotating grains. Such grains, are subjected to fast internal relaxation (Purcell 1979; Lazarian & Efroimsky 1999; Lazarian & Draine 1999b) that couples the angular momentum $\mathbf{J}$ and $\mathbf{a}_1$. As the grain slows down to thermal angular velocity, the coupling becomes weaker. As a result, $\mathbf{a}_1$ wobbles about $\mathbf{J}$ (Lazarian 1994, Lazarian & Roberge 1997). Similar to DW97, in Paper I we disregarded this effect.

Some implications of the thermal wobbling are self-evident. For instance, in Paper I we found that for a narrow

range of angles, when the radiation beam is close to being perpendicular to magnetic field, the alignment becomes "wrong" (i.e. it occurs with the maximal inertia axis *perpendicular* to the magnetic field) [5]. Such a "wrong" alignment is in contrast to what is widely observed in the ISM. However, we found that the "wrong" alignment in a diffuse medium corresponds to low angular momentum J. Therefore, we predicted in Paper I that thermal wobbling of grains would destroy the "wrong" alignment.

Qualitatively, in Paper I, we show that, in most cases, a high fraction of grains are aligned at a zero- J attractor point, assuming that $\mathbf{a}_1$ is always parallel to $\mathbf{J}$. In reality, thermal fluctuations induce the wobbling of $\mathbf{a}_1$ with respect to $\mathbf{J}$, resulting in the modification of RATs. This, in turn, changes the alignment of $\mathbf{J}$ with respect to $\mathbf{B}$. Hence, we expect grains to be trapped at attractor points with thermal angular momentum J (hereafter called low-J attractor points).

One direct consequence of being trapped at the low-J attractor point is the decrease of the degree of the alignment of grain axes with respect to the magnetic field. The degree of alignment is defined by the Rayleigh reduction factor (Greenberg 1968)

$$R = 1.5\langle\cos^2\beta\rangle - 0.5, \quad (1)$$

where β is the angle between the maximal inertia axis $\mathbf{a}_1$ and the magnetic field $\mathbf{B}$, $\langle ...\rangle$ denotes the averaging over an ensemble of grains. Because the process of internal alignment between $\mathbf{a}_1$ and $\mathbf{J}$ occurs much faster than the alignment of $\mathbf{J}$ with respect to $\mathbf{B}$, R could be approximately separated (see Lazarian 1994) as

$$R \sim \langle R(\theta)\rangle\langle R(\xi)\rangle. \quad (2)$$

Here $\langle R(\theta)\rangle$ and $\langle R(\xi)\rangle$ are given by

$$\langle R(\theta)\rangle = 1.5\langle\cos^2\theta\rangle - 0.5, \quad (3)$$

$$\langle R(\xi)\rangle = 1.5\langle\cos^2\xi\rangle - 0.5, \quad (4)$$

where θ is the angle between $\mathbf{a}_1$ and $\mathbf{J}$, and ξ is the angle of $\mathbf{J}$ and $\mathbf{B}$.

When thermal fluctuations are absent, we have a perfect alignment of $\mathbf{a}_1$ with $\mathbf{J}$, i.e. $\langle R(\theta)\rangle = 1$. Therefore the Rayleigh reduction factor depends only on the degree of alignment of $\mathbf{J}$ with $\mathbf{B}$. In the presence of thermal fluctuations, and assuming that the relaxation process obeys the normal distribution, $\langle\cos^2\theta\rangle$ is given by

$$\langle\cos^2\theta\rangle = Z\int_0^\pi \cos^2\theta\,\sin\,\theta e^{-E(\theta)/kT_d}d\theta, \quad (5)$$

where T_d is the dust temperature, $Z = \int_0^\pi \sin\,\theta e^{-E(\theta)/kT_d}d\theta$ is the normalization factor, and $E(\theta) = J^2(1+(h-1)\sin^2\theta)/2I_1kT_d$ is the kinetic energy of the spheroidal grain. Clearly, as the value of angular momentum J becomes comparable with the thermal value, $J_{th} = \sqrt{2I_1kT_d}$ where I_1 is the maximal inertia moment of the grain, the aforementioned thermal wobbling should decrease the alignment of $\mathbf{a}_1$ with $\mathbf{B}$.

On the basis of our findings in Paper I, we can qualitatively address some questions posed in WD03. What will be the effect of random collisions on grain alignment? How do suprathermal torques, for instance, torques arising from H_2 formation (Purcell 1979) influence the alignment by RATs?

We expect that grains trapped at low J attractor points, can be significantly affected by random collisions of gas atoms. When the phase trajectory map of grains has attractor points at high- J, we expect that random collisions can depopulate grains aligned at the lower attractor point, and stochastically direct grains to the high-J attractor point. As the grains with high J are immune to randomization and internal alignment for high J is close to perfect (Purcell 1979), counter-intuitively, random gaseous bombardment can *increase* the degree of alignment. However, the removal of grains from the low-J attractor points is expected to make grain alignment time dependent, althoughh the corresponding time may be long compared with other processes in the system. With regards to H_2 un-compensated torques (Purcell 1979; Lazarian 1995), because they are fixed in the grain body coordinate system, their effect depends on the flipping rate of the grains.

Obviously, at the high attractor point corresponding to $J \gg J_{th}$, the flipping rate is very low, therefore, H_2 torques act together with RATs and change the angular momentum depending upon the resurfacing process. In contrast, the grains flip fast in the process of heading to low attractor points. Assuming that the correlation time-scale is shorter than the alignment time, then grains are rapidly driven to low angular momentum at which the grain flips very fast; thus H_2 torques will be averaged out to zero (see equation 62), and could result in an additional randomization at low attractor point.

Below we test our expectations with numerics.

3 RATS AND EFFECT OF THERMAL WOBBLING

In this section we briefly discuss the general definitions of RAT components, then present methods to average the torques over free motion and thermal wobbling. We also analyze the role of the third component Q_{e3} of RATs.

3.1 RATs: spin-up, alignment and precession

Similar to Paper I, in order to easily compare our results to those in earlier works, wherever possible, we preserve the notations adopted in DW97.

As in Paper I, we consider only the anisotropic component of the radiation field, the radiative torque is then defined by

$$\mathbf{\Gamma}_{rad} = \frac{\overline{u}_{rad}a_{eff}^2\overline{\lambda}}{2}\gamma\mathbf{Q}_\Gamma(\Theta,\beta,\Phi), \quad (6)$$

where γ is the degree of radiation anisotropy, a_{eff} is the effective size of the grain (see DW96; Paper I), and $\overline{\lambda}, \overline{u}_{rad}$ are the mean wave length and mean energy density of the radiation field. The RAT efficiency vector $\mathbf{Q}_\Gamma$ is represented in the lab system $\hat{\mathbf{e}}_1, \hat{\mathbf{e}}_2$, and $\hat{\mathbf{e}}_3$

$$\mathbf{Q}_\Gamma(\Theta,\beta,\Phi) = Q_{e1}(\Theta,\beta,\Phi)\hat{\mathbf{e}}_1 + Q_{e2}(\Theta,\beta,\Phi)\hat{\mathbf{e}}_2 + Q_{e3}(\Theta,\beta,\Phi)\hat{\mathbf{e}}_3, \quad (7)$$

where Θ, β and Φ are angles describing the orientation of

[5] "Wrong" alignment without specifying the conditions for it was also reported in DW97.

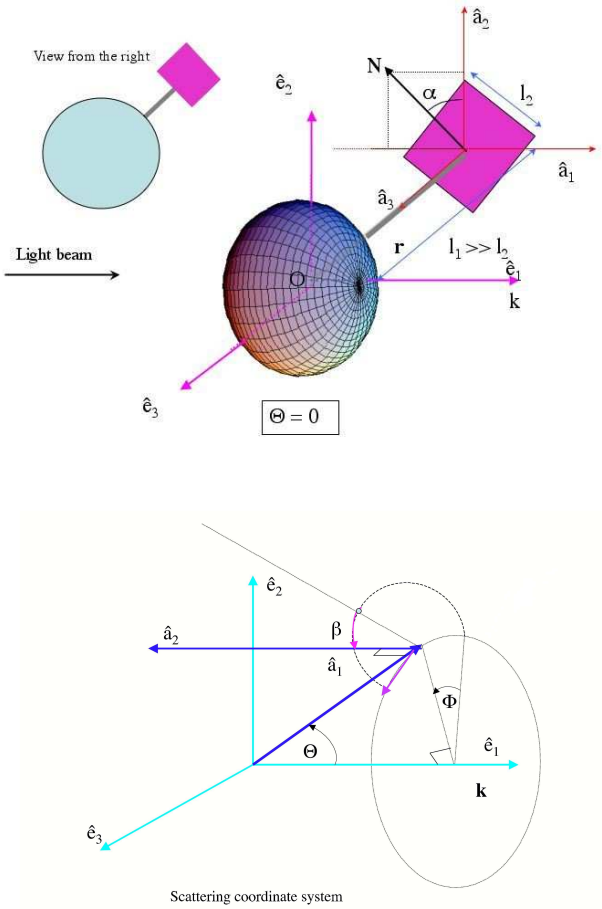


Figure 1. *Upper panel:* Geometry for AMO consisting of a perfectly reflecting spheroid and a weightless mirror. *Lower panel:* The orientation of a grain, described by three principal axes $\hat{a}_1, \hat{a}_2, \hat{a}_3$, in the laboratory coordinate system (scattering reference system) $\hat{e}_1, \hat{e}_2, \hat{e}_3$ is defined by three angles Θ, β, Φ. The direction of incident photon beam $\mathbf{k}$ is along $\hat{e}_1$.

$\mathbf{a}_1$ in the lab system (see the lower panel in Fig. 1). It was shown in Paper I that components $Q_{e1}(\Theta, \beta, \Phi = 0)$ and $Q_{e2}(\Theta, \beta, \Phi = 0)$ have universal properties and play a major role in the process of grain alignment, whereas the component $Q_{e3}(\Theta, \beta, \Phi = 0)$ does not affect either spin-up or alignment, provided that $\hat{\mathbf{a}}_1$ is coupled with $\mathbf{J}$.

Here, we only deal with the alignment of angular momentum with respect to the radiation direction or magnetic field (i.e. external alignment), therefore it is convenient to consider RATs in the spherical coordinate system J, ξ, ϕ (see Fig. 2).

In this coordinate system, the RAT can be written as

$$\mathbf{\Gamma}_{rad} = \frac{\gamma \overline{u}_{rad} a_{eff}^2 \overline{\lambda}}{2} [F(\psi, \phi, \xi)\hat{\xi} + G(\psi, \phi, \xi)\hat{\phi} + H(\psi, \phi, \xi)\hat{\mathbf{J}}], \quad (8)$$

where F, which is the torque component parallel to $\hat{\xi}$, acts to change the orientation of $\mathbf{J}$ in respect to $\mathbf{B}$; H, the component parallel to $\hat{\mathbf{J}}$, is to spin grains up and G induces the precession of $\mathbf{J}$ about the magnetic field or radiation. These

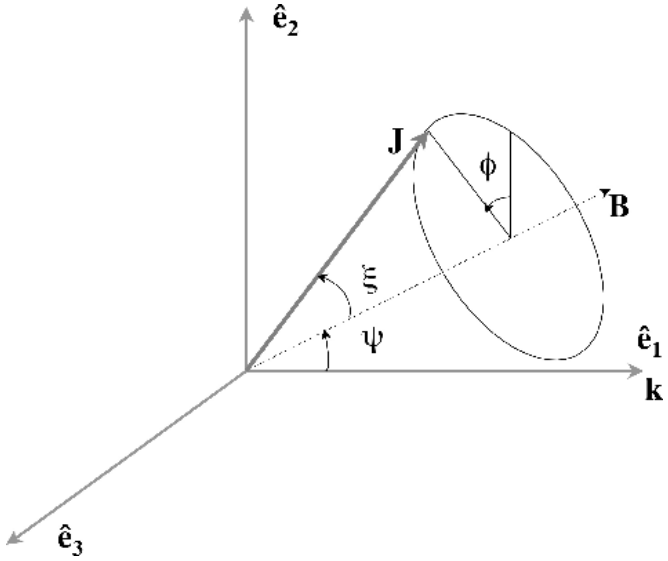


Figure 2. Alignment coordinate system in which ψ is the angle between the magnetic field $\mathbf{B}$ and the radiation direction $\mathbf{k}$, ξ is the angle between the angular momentum vector $\mathbf{J}$ and $\mathbf{B}$, ϕ is the Larmor precession angle.

are given by

$$\begin{aligned} F(\psi, \phi, \xi) &= Q_{e1}(\xi, \psi, \phi)(-\sin\psi\cos\xi\cos\phi - \sin\xi\cos\psi) \\ &+ Q_{e2}(\xi, \psi, \phi)(\cos\psi\cos\xi\cos\phi - \sin\xi\sin\psi) \\ &+ Q_{e3}(\xi, \psi, \phi)\cos\xi\sin\phi, \quad (9) \\ G(\psi, \phi, \xi) &= Q_{e1}(\xi, \psi, \phi)\sin\psi\sin\phi - Q_{e2}(\xi, \psi, \phi)\cos\psi\sin\phi \\ &+ Q_{e3}(\xi, \psi, \phi)\cos\phi, \quad (10) \\ H(\psi, \phi, \xi) &= Q_{e1}(\xi, \psi, \phi)(\cos\psi\cos\xi - \sin\psi\sin\xi\cos\phi) \\ &+ Q_{e2}(\xi, \psi, \phi)(\sin\psi\cos\xi + \cos\psi\sin\xi\cos\phi) \\ &+ Q_{e3}(\xi, \psi, \phi)\sin\xi\sin\phi, \quad (11) \end{aligned}$$

where $Q_{e1}(\xi, \psi, \phi), Q_{e2}(\xi, \psi, \phi), Q_{e3}(\xi, \psi, \phi)$, as functions of ξ, ψ and ϕ, are components of the RAT efficiency vector in the lab coordinate system (see DW97; Paper I). To obtain $Q_{e1}(\xi, \psi, \phi), Q_{e2}(\xi, \psi, \phi)$ and $Q_{e3}(\xi, \psi, \phi)$ from $\mathbf{Q}_\Gamma(\Theta, \beta, \Phi)$, which is calculated using the AMO or provided by DDSCAT for irregular grains, we need to use the relations between ξ, ψ, ϕ and Θ, β, Φ (see WD03 and Appendix A).

3.2 Free-torque motion

In the absence of external torques, a grain rotates around its principal axes. This motion is called free-torque motion. For a symmetric grain (e.g. the spheroidal body of AMO or brick; Paper I, Spitzer & McGlynn 1979), the free-torque motion consists of the nutation of angular velocity ω around $\mathbf{J}$ at a constant angle γ and the rotation around the maximal inertia axis $\mathbf{a}_1$ (see Fig. 3) with a period P_τ.

In general, an irregular grain can be characterized by an ellipsoid with moments of inertia I_1, I_2 and I_3 around three principal axes $\mathbf{a}_1, \mathbf{a}_2, \mathbf{a}_3$, respectively. For a freely rotating grain, its angular momentum is conserved (i.e., $\mathbf{J}$ is fixed in space), while the angular velocity ω nutates around $\mathbf{J}$. We can call the wobbling associated with the irregularity in the grain shape *irregular wobbling*, to avoid confusion with thermal wobbling (also thermal fluctuations) induced

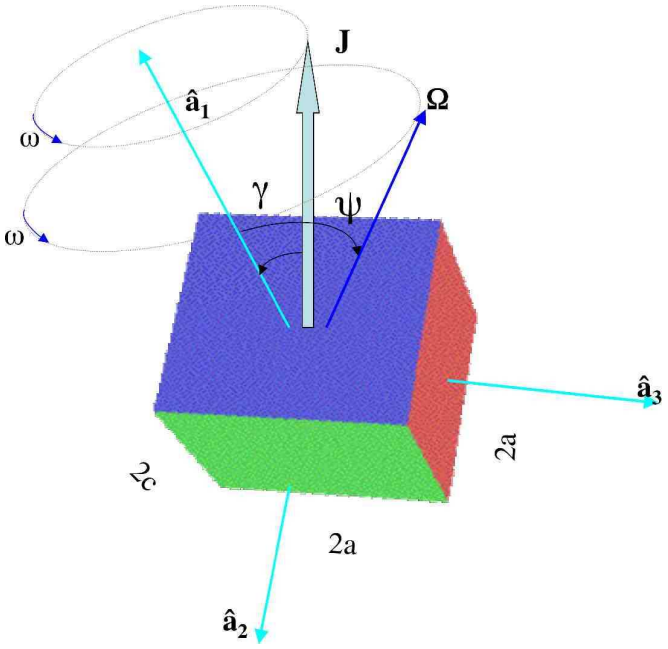


Figure 3. In body frame, the motion of a brick consists of the nutation of $\mathbf{\Omega}$ about $\hat{\mathbf{a}}_1$ and the precession of $\mathbf{J}$ around $\hat{\mathbf{a}}_1$.

by the Barnett effect (Purcell 1979) and nuclear relaxation (Lazarian & Draine 1999b).

Obviously, the time-scales of the free-torque motion (e.g. rotation period P_τ) are much shorter than other time-scales (e.g., internal relaxations and the gas damping time; see Lazarian 2007). As a result, it is always feasible to average RATs over the free-torque motion. A description of the free-torque motion for an asymmetric top in terms of Euler angles γ, α and ζ (see Fig. A1) can be found in classical textbooks (e.g. Landau & Lifshitz (1976; see also WD03). For an AMO with a spheroidal body, as in Fig. 1, the Euler angle γ is constant, while α and ζ are functions of time (see Spitzer & McGlynn 1979). For irregular grains, we can get the Euler angles by numerically solving the equations of motion (see Appendix C).

3.3 Averaging over free torque motion and role of Q_{e3}

As mentioned earlier, the rotation period P_τ about the maximal inertia axis and the precession time are both much shorter than the gas damping time. Therefore, we can average RATs over these processes.

In Figure 4 we show the phase trajectory of the tip of $\mathbf{a}_1$ about $\mathbf{J}$ for a spheroid and a triaxial ellipsoid for two initial angles $\gamma_0 = \pi/10$ and $\gamma_0 = \pi/4$. It is shown that in the case of spheroid, the trajectory is a circle corresponding to the precession of $\mathbf{a}_1$ about $\mathbf{J}$ at a constant angle γ, but the evolution of the tip of vector $\mathbf{a}_1$ produces a torus shape for the irregular grain. As a result, the average over free-torque motion for spheroid is concerned only the average over a circle, i.e. over the precession, whereas it is required to average RATs over the torus area (see Fig. 4).

The averaging algorithm over free-torque motion for triaxial ellipsoid has been realized in §3 in WD03. However, they averaged RATs over a single period of rotation P_τ.

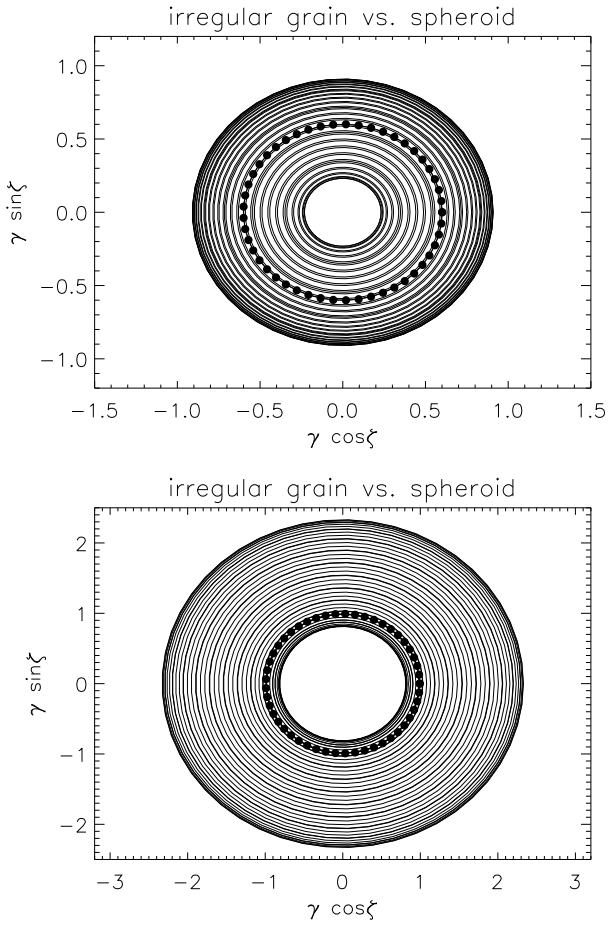


Figure 4. The evolution of the tip of the maximal inertia axis $\mathbf{a}_1$ around the angular momentum for two initial angles $\gamma_0 = \pi/10$ (*upper panel*) and $\gamma_0 = \pi/4$ (*lower panel*) of $\mathbf{a}_1$ and $\mathbf{J}$. Here ζ is the nutation angle of $\hat{\mathbf{a}}_1$ about $\mathbf{J}$ and γ is the azimuthal angle between $\hat{\mathbf{a}}_1$ and $\mathbf{J}$. Filled dots and torus show the evolution of $\mathbf{a}_1$ around $\mathbf{J}$ for the spheroid and the irregular grain respectively.

We feel that a different averaging over a longer time is appropriate. This is well motivated due to a many orders of magnitude difference of the rotation time and the time-scale of internal relaxation (see Table 1).

We compare the results obtained by averaging RATs from an AMO (see equations (23)-(25)) with the body being a triaxial ellipsoid over thermal fluctuations for time step $N = 10^2$ and $N = 10^2$ with results for $Q_{e3} = 0$ and $N = 10^2$ in Fig. 5. It can be seen that the torque components $\langle F\rangle_\phi, \langle H\rangle_\phi$ for the first and the last cases are almost the same, but their averaged torques have a small difference with those obtained in the second case. Therefore, we can expect that the contribution of Q_{e3} to the spinning and aligning torques is negligible when the averaging of RATs is performed with a sufficient accuracy (i.e. with sufficient high time step). In our study for the AMO, Q_{e3} is disregarded for both the alignment and spin-up process.

3.4 Thermal fluctuations and thermal flipping

Thermal fluctuations (i.e. thermal wobbling) and flipping arise from the coupling of rotational and vibrational degrees

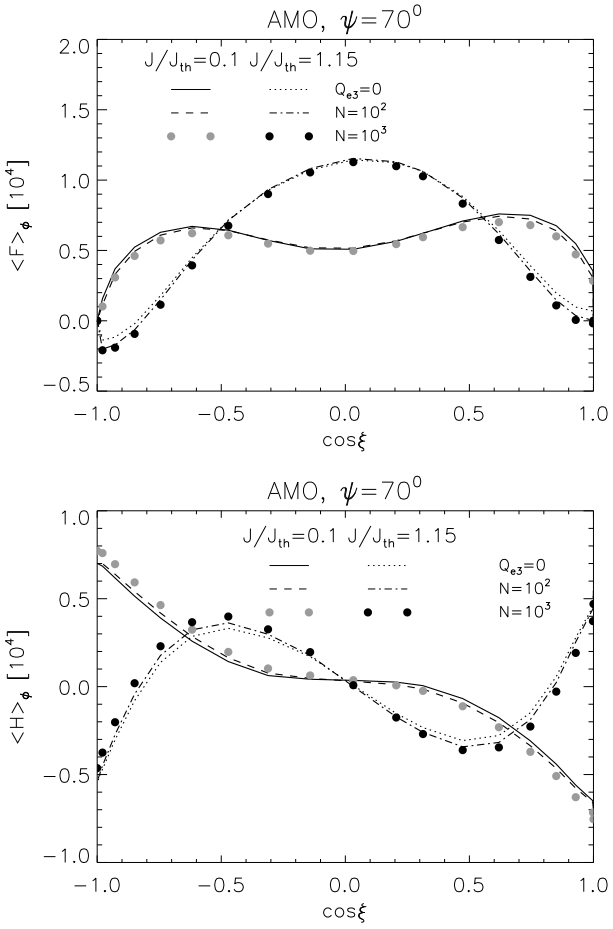


Figure 5. $\langle F\rangle_\phi$ and $\langle H\rangle_\phi$ are shown for different time-steps N of averaging and for the case $Q_{e3}=0$ corresponding to two values of angular momentum. It can be seen that the torques obtained with $N=10^3$ steps do not depend on Q_{e3}.

of freedom induced by internal relaxations. The effect was first discussed in Lazarian (1994). At that time, the strongest internal relaxation was believed to be associated with the Barnett effect (Purcell 1979).

The Barnett relaxation can be easily understood. Indeed, a freely rotating paramagnetic grain acquires a magnetic moment that is parallel to angular velocity $\mathbf{\Omega}$ due to the Barnett effect (first discussed in this context in Dolginov & Mytrophanov 1976). The Barnett effect is the phenomenon of transferring the macroscopic angular momentum of a rotating body to electrons through flipping electronic spins. To some degree, the magnetization of the rotating body is analogous with the body at rest, which is magnetized by a rotating external magnetic field. The Barnett equivalent magnetic field is $\mathbf{H}_{Be}=\mathbf{\Omega}/\gamma$ where $\gamma=e/2mc$ is the magnetogyric ratio of electrons (Purcell 1979).

Because $\mathbf{\Omega}$ may not coincide with the maximal inertia axis $\mathbf{a}_1$, it precesses continuously in the grain coordinate system (see Fig. 3). Therefore, the Barnett equivalent field can be decomposed into the constant component parallel to the precession axis and the rotating component which is perpendicular to it[6]. Apparently, the rotating component will induce a dissipation of rotational energy. As a result, we have an alignment of angular velocity and maximal inertia axis with angular momentum.

Lazarian & Draine (1999a) found a new effect related to nuclear spins, which they termed nuclear relaxation. Similar to the rearranging of electronic spins, nuclear spins also become oriented by angular momentum transferred from the body. Although the nuclear magnetization arising from grain rotation is mostly negligible compared to that arising from electrons (see Purcell 1979), the nuclear relaxation was shown to be much more efficient than Barnett relaxation for $10^{-5}<a_{eff}<10^{-4}$ cm grains. This can be easily understood. Spin flipping is a mechanical effect that depends on the angular momentum of the species rather than on their magneto-magnetogyric ratio γ. Thus, a rotating grain will have the same portion of nuclear and electron spins flipped. The magnetic field that induces such a flip is different for electrons and nuclei (i.e. it is inversely proportional to γ). The dissipation is proportional to the "equivalent" field squared (i.e. to $B_{eq}^2\sim\frac{1}{\gamma^2}$). It does not depend on the value of the nuclear magnetic moment, as the lag between magnetization and Ω increases with the decrease of the magnetic moments. In other words, the coupling between nuclear spins is less efficient than the coupling between electron spins; hence, there is a substantial lag in the nuclear spin alignment when $\mathbf{\Omega}$ precesses around $\mathbf{a_1}$. All in all, although the magnetic moment arising from nuclear spins of a rotating body is negligible, the corresponding relaxation (i.e. nuclear relaxation) is approximately 10^6 times higher than the Barnett one.

Thermal fluctuations within the grain body (see Purcell 1979) coupled via internal relaxation with the macroscopic rotation of the grain can affect the internal alignment, and result in random deviations of the major axis $\mathbf{a_1}$ in respect to $\mathbf{J}$. Following the fluctuation-dissipation theorem (Landau & Lifshitz 1976), the thermal equilibrium distribution of $\hat{\mathbf{a}}_1$ deviations can be established. The average of a torque A over thermal fluctuations for a spheroid with $I_1>I_2=I_3$ is defined by (Lazarian & Roberge 1997)

$$\langle A\rangle=\frac{\int_0^{\pi/2}d\gamma A(\gamma,J)\ \sin\gamma\exp[-E/kT_d]}{\int_0^{\pi/2}d\gamma\ \sin\gamma\exp[-E/kT_d]},\qquad(12)$$

where $h=\frac{I_1}{I_2}$, γ is the deviation angle of $\mathbf{a}_1$ and $\mathbf{J}$, and the kinetic energy E of the grain is

$$E(\gamma)=\frac{J^2}{2I_1}[1+(h-1)\sin^2\gamma].\qquad(13)$$

For irregular grains with $I_1>I_2>I_3$, the corresponding average is given in Appendix C.

Using the RAT expressions obtained for the AMO (see Paper I), one can explicitly integrate equation (12) to obtain RATs induced by thermal fluctuations. However, for irregular grains, we need to numerically average RATs according to equation (D1). The resulting averaged RAT components are plugged into equations (9-11) to obtain

[6] A more accurate description of the process that account for the finite spin-lattice relaxation is provided in Lazarian & Draine 1999b

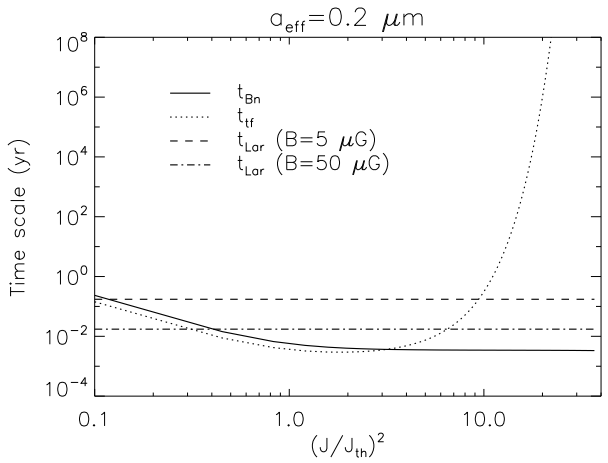


Figure 6. Larmor precession, internal relaxation and thermal flipping time-scales for $B = 5\mu G$ and $B = 50\mu G$ for a grain size of $a_{eff} = 0.2\mu m$. When magnetic field increases, the Larmor precession time-scale decreases and becomes comparable to the Barnet relaxation time-scale for small J.

$\langle F(\xi,\phi,\psi,J)\rangle, \langle H(\xi,\phi,\psi,J)\rangle, \langle G(\xi,\phi,\psi,J)\rangle$, which are required to solve the equations of motion.

The internal relaxation can induce the axis $\mathbf{a}_1$ to flip over with respect to $\mathbf{J}$. This phenomenon is called thermal flipping (Lazarian & Draine 1999a). The probability of thermal flipping has been obtained in Lazarian & Draine (1999a),

$$t_{tf}^{-1} = t_{Bn}^{-1}\exp[-0.5(\frac{J^2}{J_{th}^2} - 1)], \quad (14)$$

where $J_{th} = \sqrt{2I_1 kT_d}$ is the thermal angular momentum corresponding to the dust temperature, $t_{Bn} = (t_{Bar}^{-1} + t_{nucl}^{-1})^{-1}$ is the internal relaxation time for Barnett and nuclear relaxation processes. Because t_{nucl} is usually much shorter than t_{Bar} for grains from 10^{-5} to 10^{-4} cm, the nuclear relaxation dominates the process of thermal flipping for typical *aligned* interstellar grains (see Kim & Martin 1995).

In our analysis, we assume that thermal fluctuation and flipping time-scales are shorter than the Larmor precession time. Fortunately, for the magnetic field of the ISM and for astronomical silicate material, the Larmor precession time-scale is much longer than that of thermal fluctuations and thermal flipping. Therefore, averaging over the later motion is appropriate.

For circumstances in which magnetic field is stronger, the Larmor precession time-scale may be comparable with the thermal flipping time-scale. For instance, Fig. 6 shows that for $B = 50\mu G$ and for ordinary paramagnetic grains, $t_{Lar} \sim t_{tf}$ for $J < 10J_{th}$. For this case, in order to treat properly the grain dynamics, it is necessary to follow both the thermal fluctuation and Larmor precession.

3.5 Equations of motion

The motion of a grain subjected to a net torque is completely determined by three variables: the angle ξ between the angular momentum vector $\mathbf{J}$ and the magnetic field direction $\mathbf{B}$, the precession angle ϕ of $\mathbf{J}$ around $\mathbf{B}$ and the value of the angular momentum J (see the lower panel of Fig. 1). The equations of motion, if we *disregard paramagnetic dissipation* for these variables are

$$\frac{d\phi}{dt} = \frac{\gamma u_{\rm rad} a_{\rm eff}^2 \overline{\lambda}}{2J\sin\xi}\langle G(\xi,\phi,\psi,J)\rangle - \Omega_B, \quad (15)$$

$$\frac{d\xi}{dt} = \frac{\gamma u_{\rm rad} a_{\rm eff}^2 \overline{\lambda}}{2J}\langle F(\xi,\phi,\psi,J)\rangle, \quad (16)$$

$$\frac{dJ}{dt} = \frac{1}{2}\gamma u_{\rm rad} a_{\rm eff}^2 \overline{\lambda}\langle H(\xi,\phi,\psi,J)\rangle - \frac{J}{t_{gas}}, \quad (17)$$

where $\langle F(\xi,\phi,\psi,J)\rangle, \langle G(\xi,\phi,\psi,J)\rangle$, and $\langle H(\xi,\phi,\psi,J)\rangle$ are defined by equations (9)-(11), which are already averaged over thermal fluctuations (see WD03), t_{gas} is the gas damping time-scale (see Table 1) and Ω_B is the Larmor precession frequency of the angular momentum about the magnetic field.

For the ISM, the Larmor precession time is always shorter than the gas damping; thus, we can average equations (16) -(17) over a precession period. As a result, equations (15)-(17) can be reduced to a couple equation for ξ and J only in which the spinning and aligning torque $\langle F\rangle$ and $\langle H\rangle$ are replaced by $\langle F\rangle_\phi$ and $\langle H\rangle_\phi$, which denote the quantities obtained from averaging corresponding RATs over the Larmor precession angle ϕ from 0 to 2π.[7]

A stationary point in a phase trajectory map is determined by ξ_s, J_s, which are solutions of the equations of motion (see DW97)

$$\frac{d\xi}{dt} = 0, \quad (18)$$

$$\frac{dJ}{dt} = 0. \quad (19)$$

The above stationary point is an attractor point if

$$\frac{1}{\langle H\rangle_\phi}\frac{d\langle F\rangle_\phi}{d\xi}\bigg|_{\xi_s,J_s} < 0, \quad (20)$$

and is a repellor point otherwise (see DW97).

From equations (16) and (17), we get ξ_s, J_s that satisfy

$$\langle F(\xi_s,\psi,J)\rangle_\phi = 0, \quad (21)$$

$$J_s = t_{gas}\frac{1}{2}\gamma u_{\rm rad} a_{\rm eff}^2 \overline{\lambda}\langle H(\xi_s,\psi,J)\rangle_\phi. \quad (22)$$

4 RAT ALIGNMENT FOR AMO

We first consider the role of thermal fluctuations in grain alignment based on an AMO consisting of a reflecting spheroid ($I_2 = I_3$, hereafter *spheroidal* AMO) and a mirror as in Paper I. Then, in order to see the correspondence of the AMO with irregular grains in terms of dynamics, we replace the spheroid by an ellipsoid with the principal moments of inertia $I_1 > I_2 > I_3$ (hereafter *ellipsoidal* AMO).

[7] For the sake of simplicity, hereafter, we denote $\langle F\rangle = \langle F(\xi,\phi,\psi,J)\rangle$, $\langle H\rangle = \langle H(\xi,\phi,\psi,J)\rangle$, and $\langle F\rangle_\phi = \langle F(\xi,\phi,\psi,J)\rangle_\phi$, $\langle H\rangle_\phi = \langle H(\xi,\phi,\psi,J)\rangle_\phi$.

4.1 RATs: general expressions

In terms of RATs, an AMO is formally only applicable for $\lambda \ll a_{eff}$ as only in this case, is geometric optics approach, used to derive the analytical formulae in Paper I, appropriate. However, in Paper I we proved that the functional forms of RATs for the AMO and irregular grains for $\lambda \geqslant a_{eff}$ are similar. By choosing the appropriate ratio $Q_{e1}^{max}/Q_{e2}^{max}$ it is possible to see that the dynamics of the AMO is similar to that of irregular grains, if their torque ratio $Q_{e1}^{max}/Q_{e2}^{max}$ is the same. Therefore, the AMO can act as a proxy for actual grains, and the advantage of this is that it allows an analytical insight into grain alignment.

For an AMO in which the mirror is tilted by an angle α with the axis $\mathbf{a_2}$, the RAT components are given by (see Paper I)

$$\begin{aligned} Q_{e1}(\Theta,\beta,0) = -\frac{4l_1}{\lambda}(|n_1\cos\Theta - n_2\sin\Theta\cos\beta|[n_1n_2\cos^2\Theta \\ + \frac{n_1^2}{2}\cos\beta\sin 2\Theta - \frac{n_2^2}{2}\cos\beta\sin 2\Theta \\ - n_1n_2\sin^2\Theta\cos^2\beta]), \end{aligned} \tag{23}$$

$$\begin{aligned} Q_{e2}(\Theta,\beta,0) = \frac{4l_1}{\lambda}(|n_1\cos\Theta - n_2\sin\Theta\cos\beta|[n_1^2\cos\beta\cos^2\Theta \\ - \frac{n_1n_2}{2}\cos^2\beta\sin 2\Theta - \frac{n_1n_2}{2}\sin 2\Theta \\ + n_2^2\cos\beta\sin^2\Theta]), \end{aligned} \tag{24}$$

$$\begin{aligned} Q_{e3}(\Theta,\beta,0) = \frac{4l_1}{\lambda}(|n_1\cos\Theta - n_2\sin\Theta\cos\beta|n_1\sin\beta \\ \times [n_1\cos\Theta - n_2\cos\beta\sin\Theta]) \\ + (\frac{b}{l_2})^2\frac{2ea}{\lambda}(s^2-1)K(\Theta)\sin 2\Theta, \end{aligned} \tag{25}$$

where Θ is the angle between the axis of major inertia $\mathbf{a}_1$ and the radiation direction $\mathbf{k}$ (see Fig. 1*lower*); l_1 is the distance from the square mirror of side l_2 to the center mass, λ is the wavelength, $n_1 = -\sin\alpha, n_2 = \cos\alpha$ are components of the normal vector of the mirror in the grain coordinate system (see Fig. 1)[8], a, b are minor and major semi-axes of the spheroid, $s = a/b < 1$ and e is the eccentricity of the spheroid; $K(\Theta)$ is the fitting function (see also Paper I). As in Paper I, we treat the AMO with $\alpha = 45^\circ$ as our default model.

RATs at a precession angle Φ (see Fig. 1*lower*) are given by (see DW97)

$$Q_{e1}(\Theta,\beta,\Phi) = Q_{e1}(\Theta,\beta,0), \tag{26}$$

$$Q_{e2}(\Theta,\beta,\Phi) = Q_{e2}(\Theta,\beta,0)\cos\Phi - Q_{e3}(\Theta,\beta,0)\sin\Phi, \tag{27}$$

$$Q_{e3}(\Theta,\beta,\Phi) = Q_{e2}(\Theta,\beta,0)\sin\Phi + Q_{e3}(\Theta,\beta,0)\cos\Phi. \tag{28}$$

4.2 Alignment with respect to k

First we consider the alignment in respect to the direction of radiation $\mathbf{k}$, which also correspond to the situation when the direction of light $\mathbf{k}$ coincides with that of magnetic field $\mathbf{B}$ (i.e. $\psi = 0^\circ$).

[8] Note that RATs in equations (23-25) have opposite signs compared with those in Paper I because in Paper I we have defined $n_1 = \sin\alpha$ (i.e. we incorporated the minus sign of RATs into n_1)

4.2.1 Analytical averaging RATs for one component Q_{e1}

As discussed earlier in §3.4, Q_{e3} does not affect RAT alignment, apart from inducing the precession of angular momentum $\mathbf{J}$ about $\mathbf{k}$. Thus, the alignment problem only involves Q_{e1} and Q_{e2}. To clarify the role of the torque components, we first consider the alignment driven by the component Q_{e1} in the presence of thermal fluctuations.

For the default AMO (i.e. $\alpha = 45^\circ$), the contribution arising from the change in the cross-section is insignificant (see Fig. 6 in Paper I). Thus, we can ignore the factor $A_\perp = |n_1\cos\Theta - n_2\sin\Theta\cos\beta|$ present in equations (23)-(25). As a result, with an accuracy of 5%, equation (23) can be rewritten as

$$Q_{e1} \approx Q_{e1}^{max}[\frac{(3\cos^2\Theta - 1)}{2} + \cos\Theta\cos\beta + \sin^2\Theta\cos 2\beta], \tag{29}$$

where $Q_{e1}^{max} = \frac{-4l_1}{\lambda}n_1n_2$.

When there is incomplete alignment of $\hat{\mathbf{a}}_1$ and $\mathbf{J}$, we have

$$\cos\Theta = \cos\xi\cos\gamma - \sin\xi\sin\gamma\sin\eta, \tag{30}$$

where η is the precession angle of $\mathbf{a}_1$ around $\mathbf{J}$, γ is the angle of $\mathbf{a}_1$ and $\mathbf{J}$, and ξ is the angle between $\mathbf{J}$ and $\mathbf{B}$. In addition, β is a complicated function of Euler angles.

Substituting equation (30) into (29) and averaging the resulting expression over the precession angle η, the second and third term involved β are averaged to zero. Hence, we obtain

$$Q_{e1} \approx Q_{e1}^{max}[3(\cos^2\gamma\cos^2\xi + \frac{\sin^2\gamma\sin^2\xi}{2}) - 1]. \tag{31}$$

Using equations (12) and (13) for the expression (31) we obtain

$$\begin{aligned} \langle Q_{e1}\rangle \approx Q_{e1}^{max}\frac{\int_0^\pi d\gamma(\cos^2\gamma\cos^2\xi + \frac{\sin^2\gamma\sin^2\xi}{2} - 1)}{\int_0^\pi d\gamma\sin\gamma e^{-\frac{J^2}{J_{th}^2}[1+(h-1)\sin^2\gamma]}} \\ \times \sin\gamma e^{-\frac{J^2}{J_{th}^2}[1+(h-1)\sin^2\gamma]}, \end{aligned} \tag{32}$$

where $J_{th} = \sqrt{2I_1kT_d}$. The aligning and spin-up torque are respectively given by (see Eqs. 11-13)

$$\langle F\rangle_\phi = -\langle Q_{e1}\rangle\sin\xi, \tag{33}$$

$$\langle H\rangle_\phi = \langle Q_{e1}\rangle\cos\xi. \tag{34}$$

Hence,

$$\langle F\rangle_\phi \approx -\sin\xi Q_{e1}^{max}\frac{\sqrt{\pi}}{4}\frac{e^{(-1+h)\frac{J^2}{J_{th}^2}}(1+3\cos 2\xi)[e^{h\frac{J^2}{J_{th}^2}}\sqrt{-1+h}\frac{J}{J_{th}}}{\frac{J^2}{J_{th}^2}(-1+h)e^{-h\frac{J^2}{J_{th}^2}}Erfi(\sqrt{-1+h}\frac{J}{J_{th}})} + \sin\xi Q_{e1}^{max}\frac{e^{\frac{J^2}{J_{th}^2}}(3+2(-1+h)\frac{J^2}{J_{th}^2})]\sqrt{\pi}Erfi(\sqrt{-1+h}\frac{J}{J_{th}})}{\frac{J^2}{J_{th}^2}(-1+h)e^{-h\frac{J^2}{J_{th}^2}}Erfi(\sqrt{-1+h}\frac{J}{J_{th}})}, \quad (35)$$

$$\langle H\rangle_\phi \approx \cos\xi Q_{e1}^{max}\frac{\sqrt{\pi}}{4}\frac{e^{(-1+h)\frac{J^2}{J_{th}^2}}(1+3\cos 2\xi)[e^{h\frac{J^2}{J_{th}^2}}\sqrt{-1+h}\frac{J}{J_{th}}}{\frac{J^2}{J_{th}^2}(-1+h)e^{-h\frac{J^2}{J_{th}^2}}Erfi(\sqrt{-1+h}\frac{J}{J_{th}})} - \cos\xi Q_{e1}^{max}\frac{e^{\frac{J^2}{J_{th}^2}}(3+2(-1+h)\frac{J^2}{J_{th}^2})]\sqrt{\pi}Erfi(\sqrt{-1+h}\frac{J}{J_{th}})}{\frac{J^2}{J_{th}^2}(-1+h)e^{-h\frac{J^2}{J_{th}^2}}Erfi(\sqrt{-1+h}\frac{J}{J_{th}})} \quad (36)$$

Equation (35) reveals that $\langle F\rangle_\phi = 0$ for $\xi = 0, \pi$ and $\cos 2\xi = -1/3$, regardless of angular momentum J. In addition, zero points $\cos\xi = 0$ and $\cos 2\xi = -1/3$ of $\langle H\rangle_\phi$ do not depend on J either. This indicates that thermal fluctuations within the *spheroidal* grains do not alter the value of angular momentum (i.e. $J = 0$) at low-J attractor points produced by RATs when $J \to J_{th}$. Therefore, we expect that the resulting alignment is not significantly affected by thermal fluctuations.

The above features of RATs can be seen in Fig. 7, which shows RAT components $\langle F\rangle_\phi$ (solid line) and $\langle H\rangle_\phi$ (dashed line) as functions of ξ at a value of angular momentum $J = 0.1J_{th}$. It follows that there will be four stationary points in the phase map, corresponding to $\langle F\rangle_\phi = 0$ at $\xi = 0, \pi/3, 2\pi/3, \pi$. In addition, the stationary point $\xi = 0$ is a high-J attractor point as $\frac{d\langle F\rangle_\phi}{\langle H\rangle_\phi d\xi}\Big|_{\xi=0} < 0$ and $\langle H\rangle_\phi(\xi = 0) > 0$ (see the upper panel in Fig. 7). The lower panel of Fig. 7 shows $\langle F\rangle_\phi$ and $\langle H\rangle_\phi$ as functions of J/J_{th} for $\xi = \pi/3$. There, it can be seen that for $J \gg J_{th}$, $\langle F\rangle_\phi$ and $\langle H\rangle_\phi$ are saturated as a result of the perfect coupling of $\mathbf{a}_1$ with $\mathbf{J}$, which makes RATs independent on the angular momentum. As J/J_{th} decreases, $\langle F\rangle_\phi$ and $\langle H\rangle_\phi$ decrease steeply (see Fig. 7).

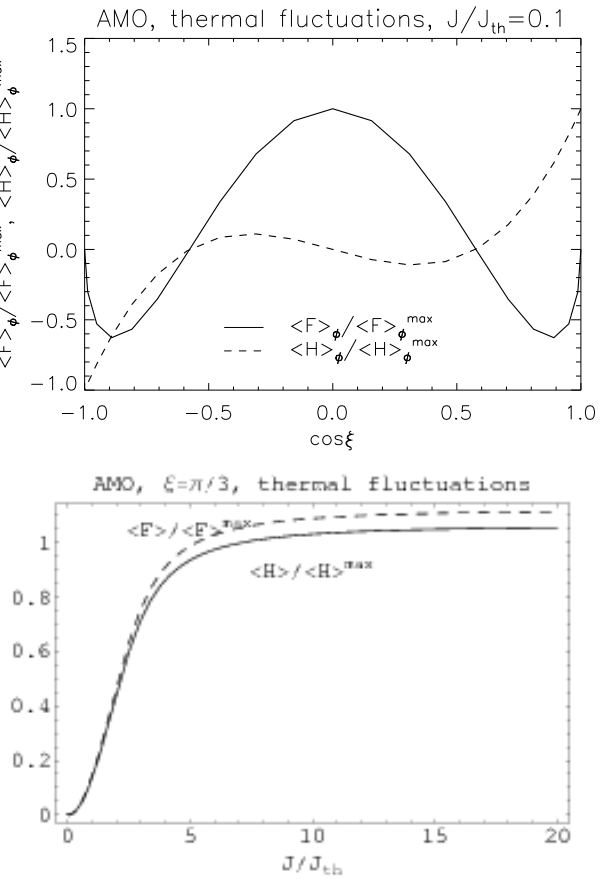


Figure 7. *Spheroidal* AMO: aligning $\langle F\rangle_\phi$ and spinning $\langle H\rangle_\phi$ torques averaged over thermal fluctuations for the case $\psi = 0°$ and $Q_{e2} = 0$. *Upper panel* shows $\langle F\rangle_\phi$ and $\langle H\rangle_\phi$ as functions of ξ for $J = 0.1J_{th}$. *Lower panel* shows that $\langle F\rangle_\phi$ and $\langle H\rangle_\phi$ for $\xi = \pi/3$, decrease rapidly with J/J_{th} decreasing and get saturated as $J/J_{th} \gg 1$.

4.2.2 Averaged RATs for both components Q_{e1}, Q_{e2}

The analytical averaging over thermal fluctuations for Q_{e2} is more complicated because of its dependence upon Φ, which is a function of Euler angles α, γ and ξ, ϕ, ψ (see equation 27 and Appendix A). Therefore, we use numerical averaging for RATs, rather than deriving analytical expressions for them. The resulting torques $\langle F\rangle_\phi, \langle H\rangle_\phi$ are used to solve the equations of motion (16)-(17).

Fig. 8 shows spin-up and alignment torques for $J = 10^{-3}J_{th}, 0.9J_{th}$ and $10J_{th}$ corresponding to cases in which thermal fluctuations are dominant, important and negligible, respectively. It can be seen that for $J \gg J_{th}$, $\langle F\rangle_\phi = 0$ for $\cos\xi = \mp 1$. It turns out that for $J \gg J_{th}$, the AMO creates only two stationary points corresponding to perfect alignment of $\mathbf{J}$ with $\mathbf{B}$. When $J = 10^{-3}J_{th}$, there are new stationary points at $\cos\xi = \pm 0.9$ corresponding to $\langle F\rangle_\phi = 0$. This means that thermal fluctuations can produce new stationary points. At the same time, the magnitude of spinning torque $\langle H\rangle_\phi$ decreases as J decreases (i.e. when thermal fluctuations increase; see Fig. 8*lower*). As a result, the alignment of grains is expected to be similar to the case without thermal fluctuations.

4.2.3 Trajectory maps

Let us consider the dynamics of the *spheroidal* AMO driven by RATs averaged over thermal fluctuations, and test the predictions using the analytical results above.

We solve the equations of motion for grains having the same initial angular momentum and uniform orientation distribution with respect to the interstellar magnetic field. Parameters necessary for calculations for the ISM conditions are given in Table 1. Phase trajectory maps are plotted in coordinates ($\cos\xi$,$J/I_1\omega_T$) where ξ is the angle between $\mathbf{J}$ and $\mathbf{B}$, and $\omega_T = \sqrt{kT_d/I_1}$. The upper and lower parts of which correspond to $\mathbf{a}_1$ initially parallel and anti-parallel to $\mathbf{J}$, respectively. For a grain size $a_{eff} = 0.2\mu m$ and shape 1 (see Fig. 15), the ISRF can produce high stationary points with $J_{high} \sim 200I_1\omega_T$ for $\psi = 0°$. To represent high and

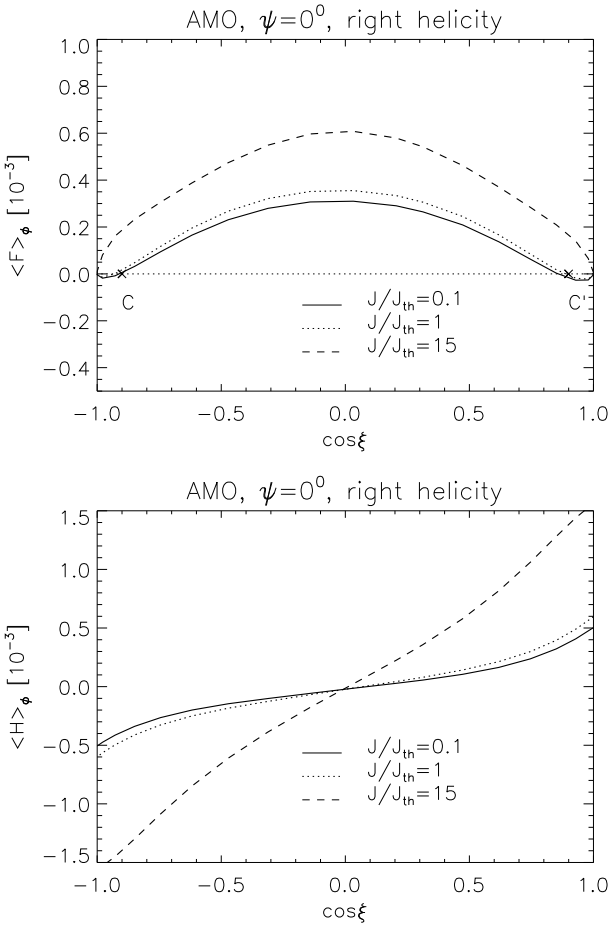


Figure 8. *Spheroidal* AMO: Aligning (*upper panel*) and spinning (*lower panel*) torques averaged over thermal fluctuations for different J/J_{th}. *Upper panel* shows that as $J = 10^{-3}J_{th}$, one new zero point of $\langle F\rangle_\phi$ appears at $\cos\xi = -0.9$. Both $\langle F\rangle_\phi$ and $\langle H\rangle_\phi$ exhibit rapid decrease with J/J_{th} decreasing.

low attractor points together, we consider the ISRF with $u_{rad} = u_{ISRF}/10$ where $u_{ISRF} = 8.64\times10^{-13} erg/cm^3$ is the energy density of the ISRF. Thus, the phase trajectory maps are shown with $J_{max} = 20I_1\omega_T$ in the present paper.

Further in the paper, a stationary point on the phase trajectory maps is marked by a circle is an attractor point, which is the point to which adjacent trajectories tend to converge, and a stationary point marked by a cross denotes a repellor point (i.e., the trajectories are repulsed while approaching it; see also Paper I).[9] In general, a phase trajectory map may have low-J and high-J attractor points or only low-J attractor points (see more in Paper I). To see clearly the modification induced by thermal fluctuations on grain dynamics, we frequently show side by side the trajectory maps for the case without thermal fluctuations as in Paper I, and with thermal fluctuations. Phase trajectory maps for the *spheroidal* AMO are shown in Figs. 9, 10 and 11 in which the upper and lower panel correspond to the cases without and with thermal fluctuations.

[9] In some trajectory maps, we do not label all existing repellor points.

Table 1. Physical parameters for diffuse ISM

Definitions	*Values*
Gas density	$\mathrm{n} = 30\ \mathrm{cm}^{-3}$
Gas temperature	$\mathrm{T_{gas}} = 100\ \mathrm{K}$
Gas damping time	$\mathrm{t_{gas}} = 4.6\times10^{12}(\frac{\hat{\rho}}{\hat{\mathrm{n}}\hat{\mathrm{T}}_{\mathrm{gas}}^{1/2}})\mathrm{a}_{-5}\ \mathrm{s}$
Dust temperature	$\mathrm{T_d} = 20\ \mathrm{K}$
Anisotropy degree	$\gamma = 0.1$
Mean wavelength	$\overline{\lambda} = 1.2\ \mu\mathrm{m}$
Mean density of theISRF	$\mathrm{u_{ISRF}} = 8.64\times10^{-13}\ \mathrm{erg\ cm}^{-3}$
Effective grain size	$\mathrm{a_{eff}} = 0.2\mu\mathrm{m}$

Here $\hat{T}_{gas} = T_{gas}/100\ K$, $\hat{n} = n/30\ g\ cm^{-3}$, and $a_{-5} = a_{eff}/10^{-5}\ cm$. $\hat{\rho} = \rho/3\ g\ cm^{-3}$ where $\rho = 3\ g\ cm^{-3}$ is the mass density of the grain.

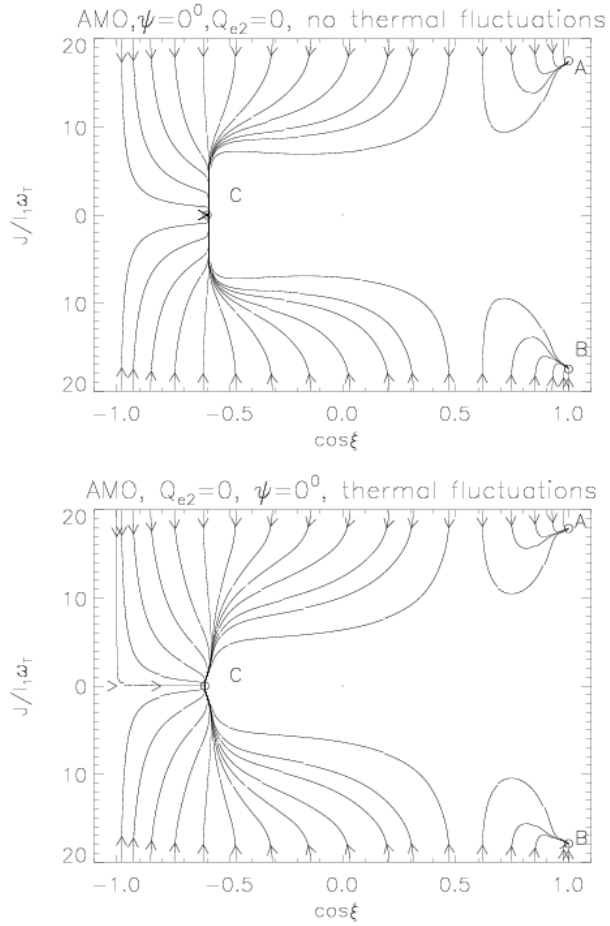


Figure 9. *Spheroidal* AMO: Phase trajectory maps for the alignment by Q_{e1} only. The upper panel shows the phase map in the absence of thermal fluctuations and the lower panel shows the phase map when thermal fluctuations are accounted for. The panels show that the position of the zero-J attractor point at $\cos\xi = -0.6$ is not changed even in the presence of thermal fluctuations.

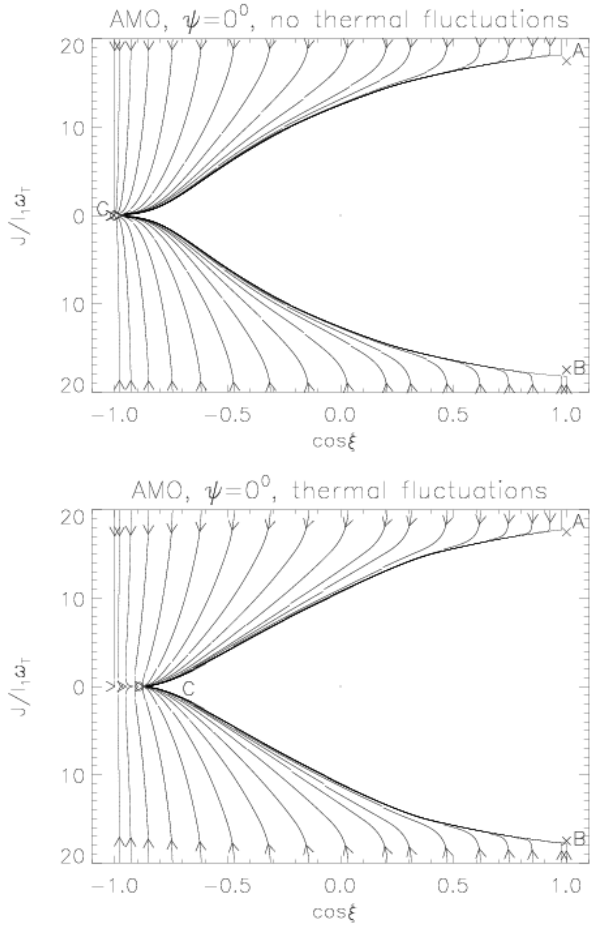


Figure 10. *Spheroidal* AMO: similar to Fig. 9, but grains are aligned by all torque components. Figs show the shift of the zero J attractor point from $\cos\xi = -1$ (*upper*) to $\cos\xi = -0.9$ (*lower*), but its angular momentum remains equal zero even when thermal fluctuations are accounted for.

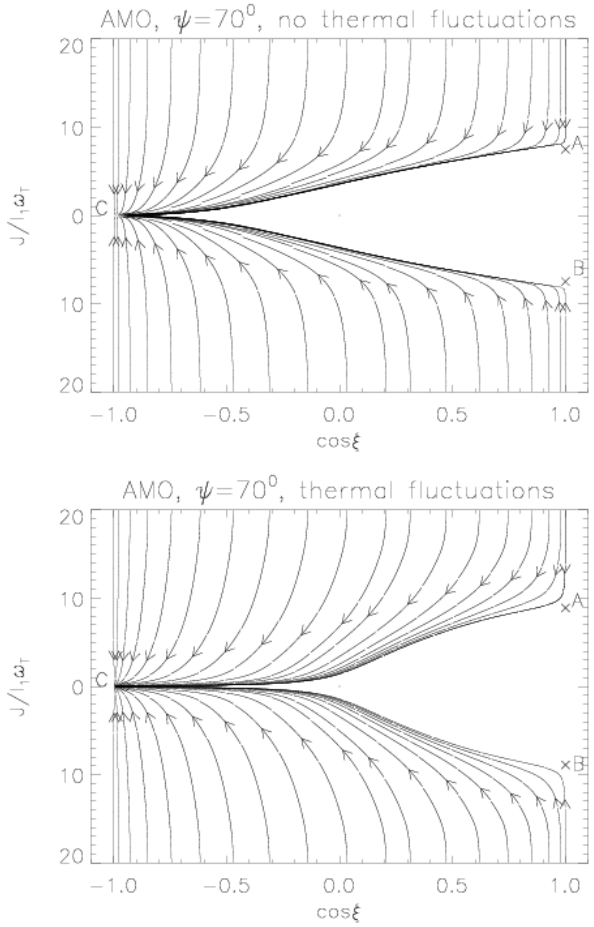


Figure 11. *Spheroidal* AMO: similar to Fig. 10, but for $\psi = 70°$. Figs show that the zero J attractor point C at $\cos\xi = -0.9$ (upper panel) panel) is unchanged in the presence of thermal wobbling (lower panel).

When the grain alignment is only driven by Q_{e1} and $\psi = 0°$ (Fig. 9), we see that each phase map has two high-J attractor points A and B. In the absence of thermal fluctuations, the torque $\langle H\rangle_\phi$ decelerates grains to the attractor point C with $J = 0$ (upper panel). When thermal fluctuations are present, the attractor point C is not affected. This result is consistent with our analytical predictions in §4.2.1

When the components Q_{e1} and Q_{e2} act together, Fig. 10 shows that the angular momentum of low attractor point remain the same (i.e. J remains equal zero). However, its position is slightly shifted to $\cos\xi = \pm 0.9$.

4.3 Alignment with respect to B

Below we consider grain dynamics when the magnetic field plays the role of alignment axis. As an example, the radiation direction $\psi = 70°$ is adopted.

Fig. 11 shows that thermal fluctuations do not increase the value of angular momentum at the attractor point C for the case $\psi = 70°$. For other angles ψ, we also found that the zero-J attractor point C is unchanged in the presence of thermal fluctuations.

It is easy to see that in the assumption of $\mathbf{a}_1 \| \mathbf{J}$, the irregular shape of the ellipsoid of inertia (i.e. $I_1 \neq I_2 \neq I_3$), is not important for the grain dynamics. However, the irregularity in the grain shape becomes important in the case of a wobbling grain because the averaging of RATs over free-torque motion (see Fig. 4) depends on its ellipsoid of inertia. To address such effects, the *spheroidal* AMO can be modified. For instance, if the mirror is not weightless, the free motion of the *spheroidal* AMO will be of a triaxial ellipsoid of inertia, rather than a spheroid. Further, in §4.4, we replace the spheroid of the AMO by a triaxial ellipsoid.

4.4 Alignment for an *ellipsoidal* AMO

In this section, we study the alignment of the *ellipsoidal* AMO in which the spheroid body (see Fig. 1) is replaced by an ellipsoid with moments of inertia $I_1 : I_2 : I_3 = 1.745 : 1.62 : 0.876$, which is similar to shape 1 (see Fig. 15).

We recall that stationary points, which determine the alignment of grains correspond to $\langle F\rangle_\phi = 0$ (see equation 22). Fig. 12 shows the torque components for $\psi = 70°$. It can be seen that for $J \gg J_{th}$ (i.e., thermal fluctuations are negligible), $\langle F\rangle_\phi = 0$ for $\cos\xi = \mp 1$. This indicates that the *ellipsoidal* AMO produce two stationary points corre-

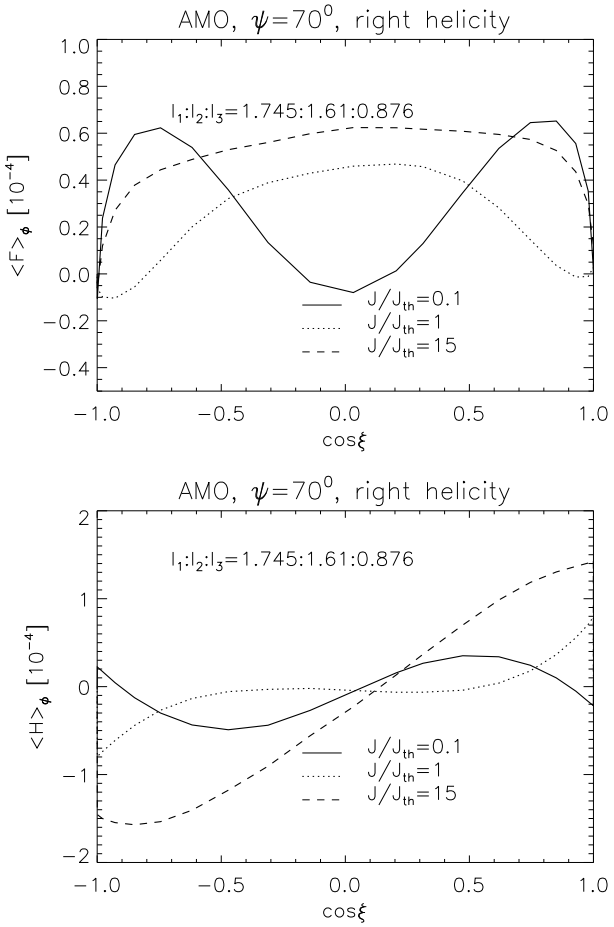


Figure 12. *Ellipsoidal* AMO: aligning and spinning torques averaged over thermal fluctuations as a function of ξ for several angular momenta. *Upper panel* shows that as $J = 1J_{th}$, one new zero point of $\langle F\rangle_\phi$ appears at $\cos\xi = -0.8$. While the change in sign of $\langle H\rangle_\phi$ in the vicinity of $\cos\xi = -1$ for $J = 0.1J_{th}$ is shown in lower panel.

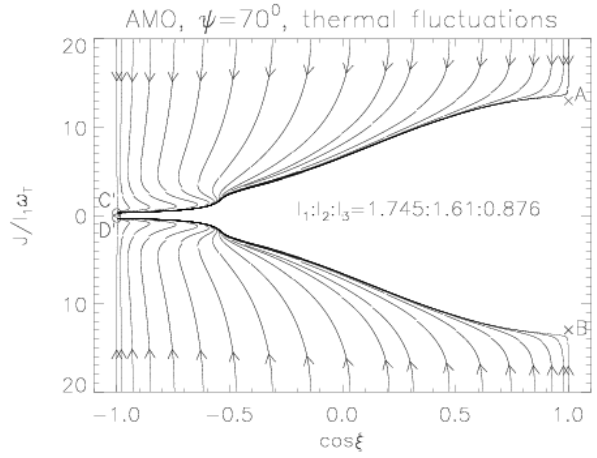


Figure 13. *Ellipsoidal* AMO: the phase map for $\psi = 70°$ shows two low attractor points C' and D' with $J = 0.5I_1\omega_T$ and two repellor points A and B.

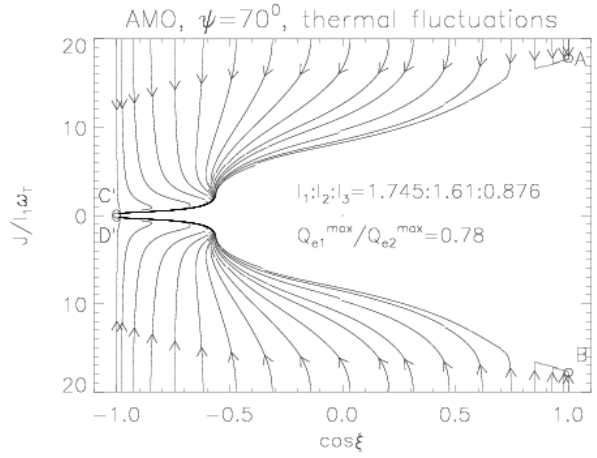


Figure 14. *Ellipsoidal* AMO: the phase map when the torque ratio $Q_{e1}^{max}/Q_{e2}^{max}$ is changed to the default value to 0.78 for $\psi = 70°$ shows two low attractor points with $J = 0.5J_{th}$ and two high J attractor points A and B with $J = 18J_{th}$.

sponding to perfect alignment of **J** with **B**. As $J \to 0.1J_{th}$, there appears a new stationary point at $\cos\xi = -0.8$. It means that thermal fluctuations produce a new stationary point at $\cos\xi \sim -0.8$. However, this new stationary point is a repellor point as $\frac{d\langle F\rangle_\phi}{\langle H\rangle_\phi d\xi}\Big|_{\cos\,\xi_s=-0.8} > 0$ (see Fig. 12). In addition, the lower panel shows the change in sign of the spinning torque from negative to positive as $J \sim 0.1J_{th}$ for $\cos\xi \sim -1$. Thus, the stationary point $\cos\xi = -1$ is an attractor because $\frac{d\langle F\rangle_\phi}{\langle H\rangle_\phi d\xi}\Big|_{\cos\,\xi_s=-1} < 0$ (see Fig. 12). Therefore, thermal fluctuations within the *ellipsoidal* AMO modify the properties of RATs as $J \to 0$, and split a zero-J attractor point in absence of thermal wobbling into two low-J attractor points. The corresponding trajectory maps for this case are shown in Fig. 13

Now we rescale the amplitude of Q_{e1}, Q_{e2} so that $Q_{e1}^{max}/Q_{e2}^{max} = 0.78$. For this AMO, Paper I shows that the grains are aligned with two high-J attractor points and a zero-J attractor point. However, in presence of thermal fluctuations and for the *ellipsoidal* AMO with $I_2 \neq I_3$, the zero-J attractor point becomes the attractor points with the value of angular momentum of the order of thermal value, as seen in Fig. 14.

5 RAT ALIGNMENT FOR IRREGULAR GRAINS

5.1 Properties of averaged RATs

We use the publicly available DDSCAT code (Draine & Flatau 2004) to calculate RATs for irregular grains (i.e. shape 1 and 3; see Fig. 15). The optical constant function for astronomical silicate is adopted (Draine & Lee 1984). We computed RAT efficiency $\mathbf{Q}_\lambda(\Theta, \beta, \Phi)$ in the lab coordinate system (see Fig. 1), over 32 directions of Θ in the range $[0, \pi]$ and 33 values of β between 0 and 2π for $\Phi = 0$ (angle produced by $\mathbf{a}_1$ and the plane $\hat{e}_1, \hat{e}_3$ where $\hat{e}_i$ are three unit vectors of the lab coordinate system; see Fig. 1). The RAT efficiency $\mathbf{Q}_\lambda(\Theta, \beta, \Phi)$ for an arbitrary angle Φ is eas-

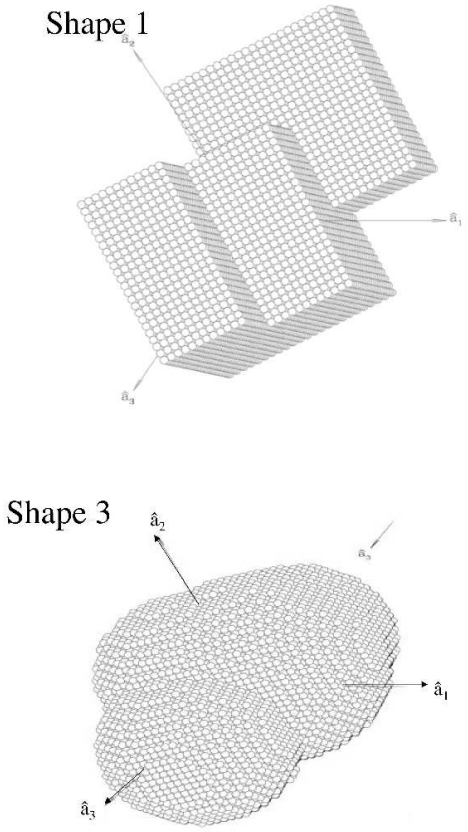


Figure 15. Irregular grains of shape 1 and shape 3 (see DW97) are taken to study RAT alignment by DDSCAT.

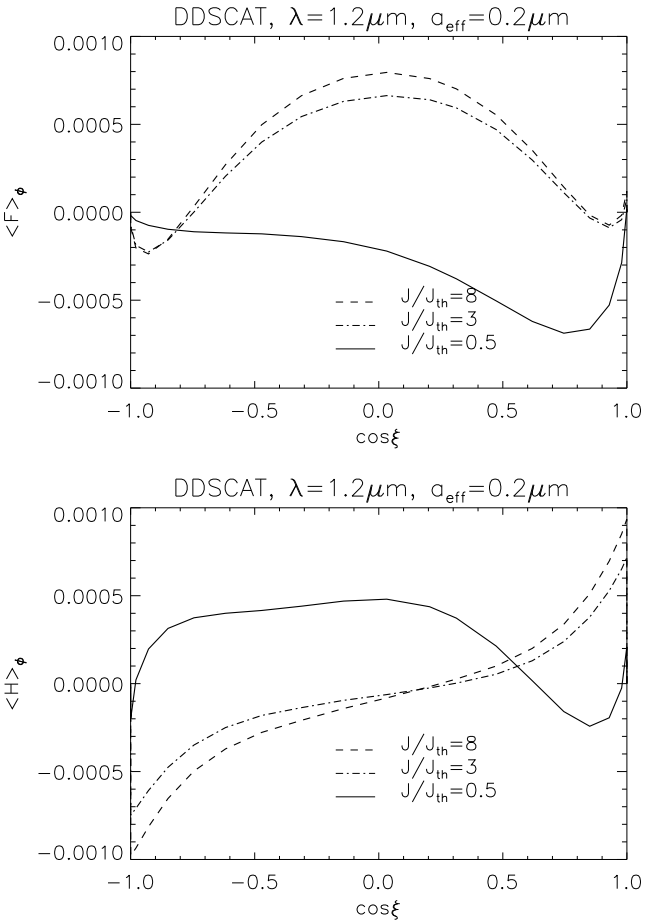


Figure 16. $\langle F\rangle_\phi$ and $\langle H\rangle_\phi$ for the monochromatic radiation field at $\psi = 70^\circ$ as functions of the angle ξ between **J** and **B** for three values of J.

ily calculated using equations (26)-(28). In our paper, we calculate RATs for irregular grains of size $a_{eff} = 0.2\mu m$ induced by monochromatic radiation field of $\lambda = 1.2\mu m$ and the spectrum of the ISRF (see Mathis et al. 1983).

Fig. 16 show $\langle F\rangle_\phi$ and $\langle H\rangle_\phi$ (i.e., aligning and spinning torques) obtained by averaging the corresponding expressions (see equations 9 and 11) over thermal fluctuations for different angular momenta, and for the monochromatic radiation at angle $\psi = 70^\circ$ toward **B**.

From Fig. 16 we see that for $J/J_{th} \gg 1$, $\langle F\rangle_\phi = 0$ at $\cos\xi = \pm 1, -0.65$, corresponding to three stationary points. However, when J/J_{th} decreases (i.e., thermal fluctuations become stronger), the intermediate stationary point shifts to the left, and disappears as $J/J_{th} \to 0$.

Fig. 17 is similar to Fig. 16, but presents torques for the entire spectrum of the ISRF and $\psi = 0^\circ$. It is also seen that the intermediate stationary point (i.e. point with $\langle F\rangle_\phi = 0$) shifts to the left as J/J_{th} decreases. It disappears when $J/J_{th} = 0$. Furthermore, following both Fig. 16 and 17 (lower panels), we see that the spinning torque $\langle H\rangle_\phi$ decreases with J decreasing. This is because for low angular momentum, thermal fluctuations become stronger, so the axis of grain $\mathbf{a}_1$ fluctuates with a wider amplitude around **J**. As a results, RATs decrease (see analytical results for the *spheroidal* AMO in the upper panel of Fig. 7).

Now let us consider the property of the intermediate zero point of the aligning torque $\langle F\rangle_\phi$ shown in the lower panel of Fig. 17. We can check that this stationary point corresponding to $J/J_{th} \sim 2.5$ is an attractor point. According to equation (20), the criteria in order for one stationary point to be an attractor point is $\frac{d\langle F\rangle_\phi}{\langle H\rangle_\phi d\xi}\Big|_{\xi_s} < 1$. With the stationary point at $\cos\xi_s = -0.85$, we have $\langle H\rangle_\phi > 0$ (see the upper panel), and $\frac{d\langle F\rangle_\phi}{d\xi}\Big|_{\xi_s} < 0$ due to the decrease of $\langle F\rangle_\phi$ with ξ in the vicinity of ξ_s (see the upper panel of Fig. 17). Thus, $\frac{d\langle F\rangle_\phi}{\langle H\rangle_\phi d\xi}\Big|_{\xi_s} < 0$, which satisfies the criteria for an attractor point.

5.2 Phase Trajectory Maps for shape 1

Let us consider the trajectory map for grains of size $a_{eff} = 0.2\mu m$ driven by RATs produced by a monochromatic radiation of $\lambda = 1.2\mu m$, in the direction $\psi = 70^\circ$, which is similar to the setting in WD03. As we mentioned above, an important difference in our treatment and that in WD03 is that we average RATs over 10^3 rotation periods rather than over only one period as WD03 did. As we discussed in §3.3,

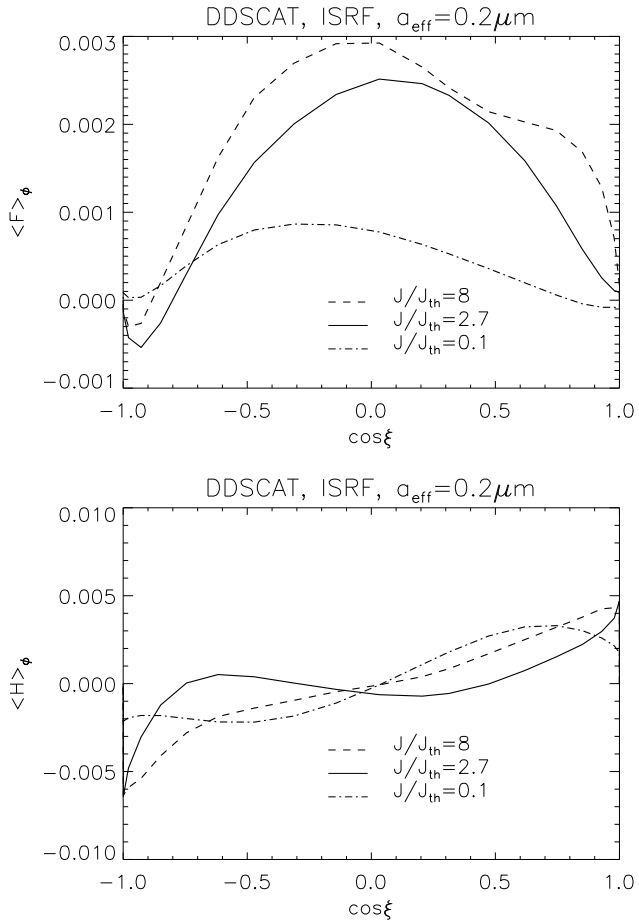


Figure 17. $\langle F\rangle_\phi$ and $\langle H\rangle_\phi$ for the ISRF at $\psi = 0°$ as functions of the angle ξ between **J** and **B** for three values of J.

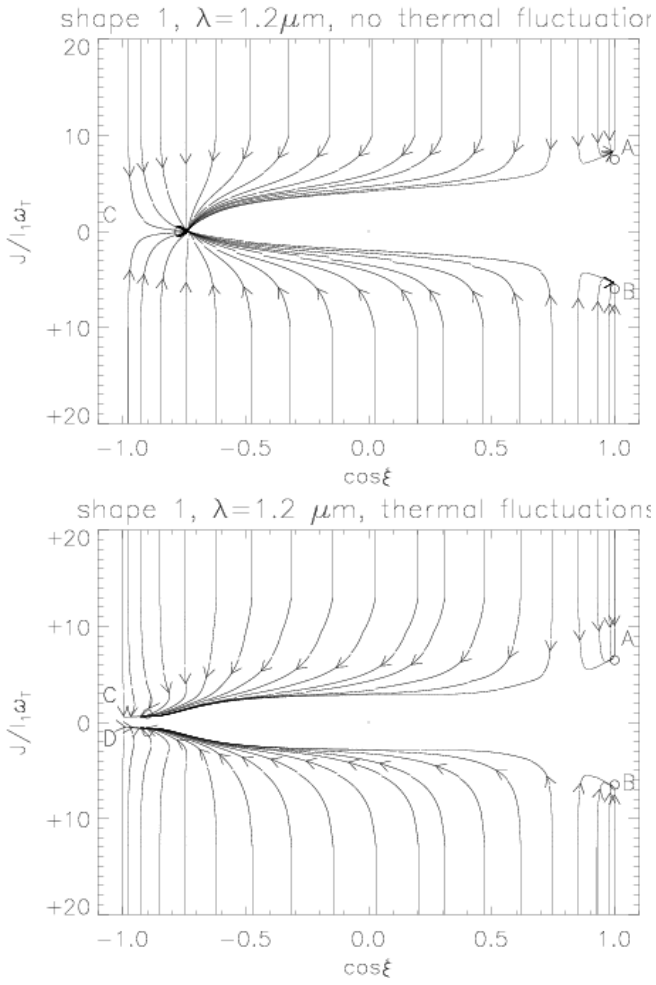


Figure 18. Phase trajectory maps for $\lambda = 1.2\mu m$ and $a = 0.2\mu m$, and $\psi = 70°$ corresponding to no thermal fluctuations (*upper panel*) and with thermal fluctuations (*lower panel*). For the case in which **J** is fixed, when grains are driven to the crossover $J = 0$, $\mathbf{a}_1$ flips over. So grains change frequently their states corresponding to switching between the upper and lower frame in the map.

one of the consequences of this is that the contribution of Q_{e3} component vanishes for aligning and spinning torque components.

The upper panel in Fig. 18 shows the trajectory map for the case without thermal fluctuations with two high-J attractor points (A, B) and one zero-J attractor point C. When thermal fluctuations are accounted for, the lower panel reveals the split of the attractor point C to C' and D' as also seen in WD03. However, the value of angular momentum at C' and D' is $J = 0.7J_{th}$, which is lower that the value obtained by WD03. This difference stems from the fact that the contribution of Q_{e3} to the spinning and aligning torques is completely canceled when we average RATs over a sufficiently long time. In fact, we tested that, if Q_{e3} is set to zero, the resulting map is the same with the lower panel of Fig. 18. Yet, if we adopt the same averaging as in WD03, we also get the low attractor point with similar value J as in WD03. We also see a correspondence between our results here with those obtained with the AMO (see §4.4).

The lower panel in Fig. 18 also shows that about 20% of grains are aligned at two high-J attractor points A, B, and about 80% grains are driven by RATs to the low-J attractor points C and D. There, grains flip to the opposite flipping state (i.e. from upper to lower frame) and back. However, immediately after entering the opposite flipping state, grains are decelerated by RATs to that point again and they flip back. So grains flip back and forth between C and D. In fact, C and D are indistinguishable because grains flip very fast between them with the probability of finding grains on each point is ~ 0.5. In that sense, the points C and D are also crossover points.[10]

Figs 19 and 20 show the phase maps of grain alignment for the full spectrum of the ISRF instead of monochromatic radiation, and for two directions of radiation $\psi = 0°$ and $90°$. For the direction $\psi = 0°$, the map in the lower panel consists of three attractor points A', B', C in which the point C is the old attractor point at very high angular momentum, and A', B' are low-J attractor points originated from A and B at $J = 0$ for the case of no thermal fluctuations (see the upper panel). In other words, averaging over thermal fluctuations

[10] These crossover points are different from those described in DW97, in which the grains were spinning up right after crossover. This stems from inaccurate treatment of crossovers in DW97, see more detail in Paper I.

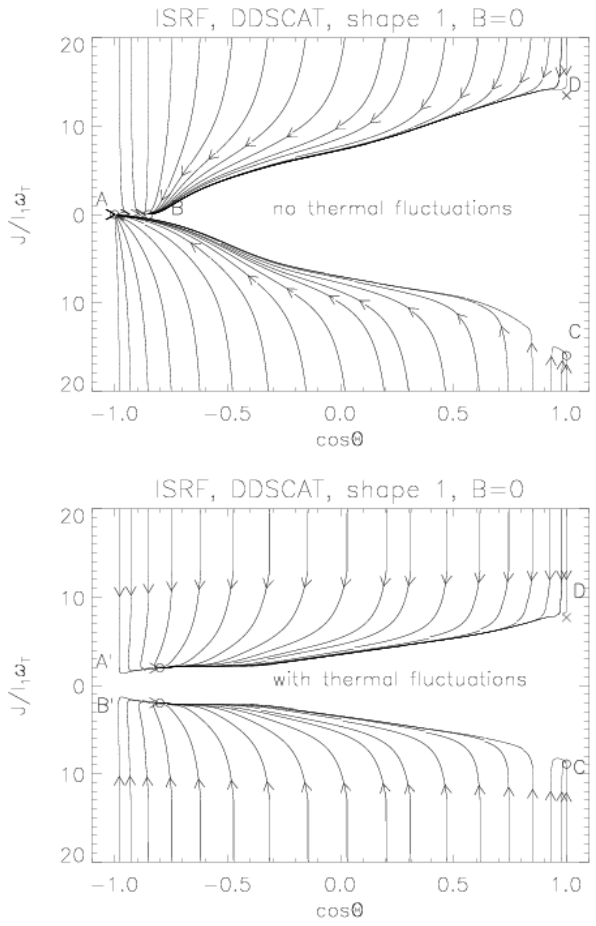


Figure 19. Trajectory maps for the entire spectrum of the ISRF and irregular grain of size $a_{eff} = 0.2\mu m$ when thermal fluctuations are absent (upper panel) and when thermal fluctuations and thermal flipping are included (lower panel), corresponding to the alignment with respect to $\mathbf{k}$ or $\psi = 0°$ (equivalent to the grain alignment in the absence of magnetic field).

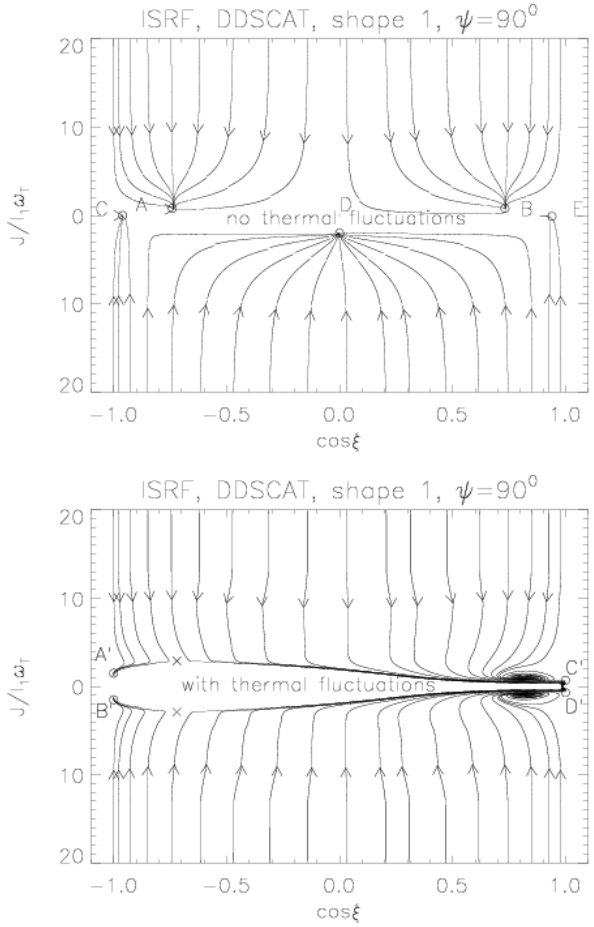


Figure 20. Similar to Fig. 19, but for $\psi = 90°$. *Upper panel*: the map with two high J attractor point A, B, two zero-J attractor points C, E and a "wrong" attractor point D at $\cos\xi = 0$. *Lower panel*: with thermal fluctuations and the "wrong" attractor point D disappears.

of grains for the ISRF and $\psi = 0°$ also changes the zero-J attractor point to the new thermal J attractor point.

In Paper I we pointed out that at ψ close to 90° for both the AMO and irregular grains, the grain alignment tends to take place with $\mathbf{a}_1 \perp \mathbf{B}$, which is in contrast to the classical Davis-Greenstein (1951) expectations. We termed this "wrong" alignment. An attractor point D at "wrong" alignment angle (i.e. $\xi = 90°$) shown in Fig. 20*upper* for the direction $\psi = 90^0$ together with four other attractor points A, B, C and E, in the absence of thermal wobbling (see also Paper I). However, in the presence of thermal wobbling, the "wrong" attractor point D is no longer existing. Instead, we obtain four new attractor points A', B', C' and D', corresponding to $J \sim J_{th}$ and $\cos\xi = \pm 1$ (see the lower panel in Fig. 20). It means that the "wrong" alignment is indeed eliminated by averaging induced by thermal wobbling (see also §2).

5.3 Dynamics of shape 3

For the sake of completeness, let us study the effect of thermal fluctuations on RAT alignment for another irregular grain (shape 3 in DW97). As an example, we consider a particular grain size $a_{eff} = 0.2\mu m$ and one light direction $\psi = 70°$.

Fig. 21 shows the trajectory maps obtained for this grain corresponding to the case without (upper panel) and with thermal fluctuations (lower panel). It is shown that for $\psi = 70°$, this grain produces a phase map with two high-J attractor points A, B and two low-J attractor points C' and D' in the presence of thermal fluctuations (see lower panel of Fig. 21). The lifting of the low-J attractor point C (see the upper panel of Fig. 21) from $J = 0$ to $J = 2J_{th}$ (C', D') when thermal fluctuations are taken into account, is also seen for this shape. However, grains can rapidly flip back and forth between C' and D'.

6 LOW J ATTRACTOR POINTS

Our study indicates that a high fraction of grains are aligned at low-J attractor points. Therefore, the origin and stability of this low-J attractor point are important for grain alignment. We address these questions below.

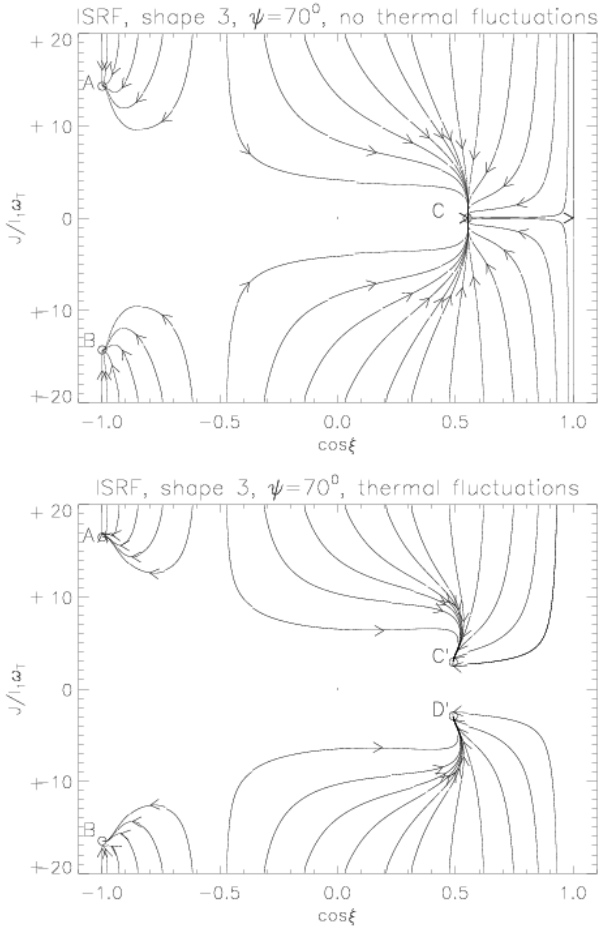


Figure 21. Phase maps for the grain shape 3 and the ISRF with two high-J attractor points corresponding to the cases without thermal fluctuations (*upper panel*) and with thermal fluctuations (*lower panel*). Thermal fluctuations shift the zero-J attractor point C to C', D' with $J = 2J_{th} = 2I_1\omega_T$.

6.1 Origin

The results above show that thermal fluctuations produce a new low-J attractor point from the zero- J attractor point, for both the ellipsoidal AMO and irregular grains, but this effect has not been seen for the *spheroidal* AMO. Now let us explain why this occurs by using the AMOs, but the explanation can be applicable to irregular grains.

First of all, let us study RATs averaged over the free-torque motion for the *spheroidal* and *ellipsoidal* AMOs. Following equation (D1) (see Appendix D), the average over thermal fluctuations can be rewritten as

$$\langle A\rangle \sim \int_0^1 ds A e^{(-q\frac{J^2}{J_{th}^2})}, \quad (37)$$

where A is the torque component that arises from the average over free-torque motion and $q = 2I_1E/J^2$ with E is the total kinetic energy. It is convenient to define

$$A(s,J) = Ae^{(-q\frac{J^2}{J_{th}^2})}, \quad (38)$$

which represents the torque resulting only from the average over free-torque motion as a function of J and the density of states in phase space s (see Appendix D).

In Fig. 22 we show torque components defined by equation (38) for *spheroidal* and *ellipsoidal* AMOs with $J = 10J_{th}$ and $J = 0.5J_{th}$, corresponding to cases in which the role of thermal fluctuations is marginal and important, respectively.

It can clearly be seen that for $J = 10J_{th}$ (i.e. $J \gg J_{th}$), the obtained torques are nearly similar for irregular and axisymmetric grains. Yet the torques drop very rapidly to zero as s (note that $s = \sin\gamma$ for the spheroid) increases (see dashed lines in Fig. 22). The former stems from the fact that for the suprathermal rotation, a good coupling between the maximal inertia axis and the angular velocity is achieved. Therefore, there is no difference between the free-motion of an irregular and axisymmetric grains.

However, the averaged torques become very different as J decreases. In fact, Fig. 22 (see the curves with $J = 0.5J_{th}$) reveal that for axisymmetric grains, RATs decrease regularly with respect to s. Whereas, RATs for irregular grains drop rapidly, change the sign and rise again with s increasing.

The effect of such a variation on the average of RATs over thermal fluctuations (see equation 37) is evident. In Fig. 23 we show the corresponding torque components $\langle F\rangle_\phi$ and $\langle H\rangle_\phi$ obtained by averaging F and H using equation (37), as functions of J for several angles ξ between $\mathbf{J}$ and $\mathbf{k}$ for $\psi = 0^\circ$. It can be seen that for $J \gg J_{th}$, the averaged torques of irregular grains are similar with those of axisymmetric grains, and they become saturated in both cases. However, their averaged torques become very different when J decreases. For instance, the averaged torques for the former case change their sign at $J \sim J_{th}$, while the torques for the later case do not. We note that for the angle $\cos\xi < 0$, the torque $\langle H\rangle_\phi$ is negative (i.e. torques tend to drive grains to zero-J attractor point) for $J \gg J_{th}$, equivalent with the absence of thermal fluctuations. As a result, the change of sign of $\langle H\rangle_\phi$ for $J \sim J_{th}$ in the presence of thermal fluctuations reveals that grains can be spun up again for $J \sim J_{th}$. To some value of J, $\langle H\rangle_\phi$ continues to reverse its sign, and grains are decelerated. In other words, the irregular grains can be aligned at low attractor points with angular momentum $J \sim J_{th}$.

Consider now a stationary point ξ_s. As discussed previously, the stationary point ξ_s is either an attractor or a repellor point depending on the sign of the spin-up torque and the derivative of the alignment torque at that point; it is an attractor point if $\frac{1}{\langle H\rangle_\phi}\frac{d\langle F\rangle_\phi}{d\xi}\Big|_{\xi_s} < 0$. Therefore, the change in sign found above for $\langle F\rangle_\phi$ and $\langle H\rangle_\phi$ can give rise to the thermal attractor points observed in maps for the *ellipsoidal* AMO and irregular grains .

In summary, the analytical analysis for the AMO results indicate that as thermal fluctuations become more important (i.e. J small), RATs as a function of ξ can have different forms (sign and magnitude) that increase the angular momentum of the low attractor points from $J = 0$ to $J \approx J_{th}$. We also see a radical difference between torques averaged over free precession of spheroidal and the free wobbling of ellipsoidal grains.

6.2 Stability of low and high-J attractor points

From Section 6.1, we see that the effect of thermal fluctuations on RATs is to produce attractor points at low J. In addition, there are also attractor points at high J to

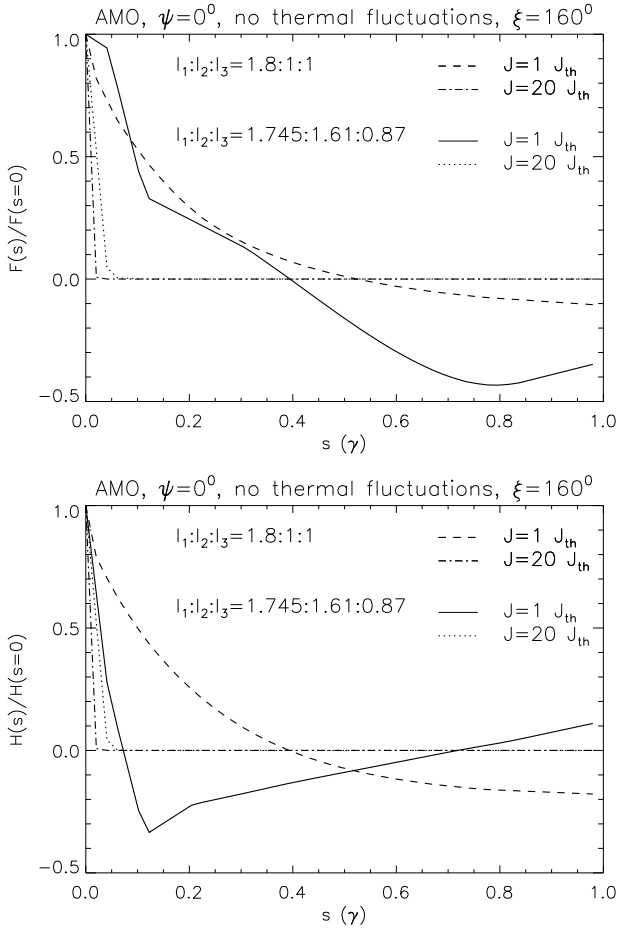


Figure 22. Spin-up and alignment torques as functions of $s(\gamma)$ for two values of angular momentum $J = 20J_{th}$ and $J = J_{th}$ corresponding to an angle $\xi = 160^{\circ}$ between angular momentum and the magnetic field, and the precession angle $\phi = 180^{\circ}$. The fast drop of F and H for small J is observed that gives rise to the fact that the sign of their averaged value over s is opposite to its sign at $s = 0$.

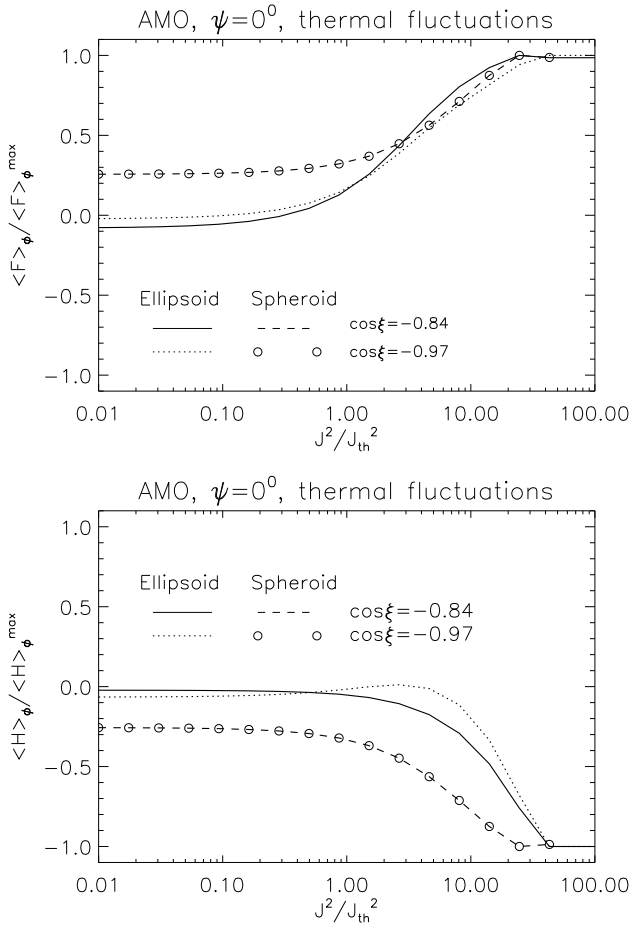


Figure 23. Aligning $\langle F\rangle_{\phi}$ and spinning $\langle H\rangle_{\phi}$ torque components averaged over the Larmor precession angle ϕ and thermal fluctuations (i.e. over s using equation 37), normalized over their amplitude values for three angles ξ, as functions of angular momentum for the spheroid and ellipsoid AMOs. Plots show the change of sign of both torques when J^2/J_{th}^2 decreases (i.e., thermal fluctuations increase) for the ellipsoid AMO, but not seen for spheroid. For $J \gg J_{th}$, the torques are constant.

which thermal fluctuations have marginal influence. It can be shown that most of grains in the ensemble tend to get in low-J attractor points. However, having low J, they may be significantly influenced by randomization processes (e.g. collisions by gaseous atoms).

For high-J attractor points present in the trajectory map (see Figs 9, 14 and 18), the angular momentum is determined by the radiation energy density u_{rad} (see equation 22), that is $J/I_1\omega_T \sim u_{rad}\langle H\rangle_{\phi}$. As a result, depending on the distance to a given radiation source, the angular momentum of the high-J attractor points changes.

However, for low-J attractor points, because the angular momentum depends on thermal fluctuations (see Hoang & Lazarian, in preparation), it does not change when radiation intensity varies. So grains of the same size, near and far from the pumping source, have low-J attractor points of similar angular momentum. Therefore, due to thermal wobbling (see Lazarian 1994), even near the radiation source, the alignment degree is not high for the case of trajectory maps without high-J attractor point. Consequently, even in regions close to the strong radiation source (e.g., star forming regions) most of grains may rotate rather slowly.

Furthermore, the angular momentum of low attractor points depends on the grain size a_{eff} because internal relaxations are a function of a_{eff} (scales as a_{eff}^7; see also Table 1). So we expect that for large grains that have weak internal fluctuations, the value of angular momentum at low-J attractor points is very close to zero as a result of the deceleration action of RATs. In contrast, small grains having strong internal relaxations, can have low-J attractor points of higher angular momentum.

7 CROSSOVER DYNAMICS

7.1 Description

The randomization of grains during crossovers has been studied by Spitzer &McGlynn (1979) and Lazarian & Draine (1997). In Paper I we studied the crossover for a *spheroidal* AMO. It is shown that grains move to the attractor point

$\cos\xi = -1, J = 0$ while undergoing multiple crossovers. In this section, we first consider large grains, so that $t_c < t_{Bar}$ and thermal flipping is not important for both axisymmetric and irregular grains. Therefore, we can solve the equations of motion for both J, ξ and the component $J_\parallel$ of $\mathbf{J}$ along $\mathbf{a}_1$. Then we incorporate the thermal fluctuations and thermal flipping into our treatment.

In Paper I, to simplify our treatment, we disregarded all internal relaxation processes during the crossover. This is justifiable as for $a_{eff} \gg a_c$ the crossover occurs on the time scale shorter than the internal (e.g.Barnett and nuclear) relaxation time. However, for typical interstellar grains with $a_{eff} < a_c$, thermal flipping occurs very fast, and thus it must be taken into account. Because the mirror is assumed to be weightless, for the *spheroidal* AMO, the dynamics of free rotation coincides with that of a spheroid. As a result, for a given J, $\mathbf{a}_1$ precesses around $\mathbf{J}$ with a constant angle γ. The state of the grain is completely determined by describing $\mathbf{J}$ in the lab and body systems. Equations of motion for this case are (see Paper I)

$$\frac{d\mathbf{J}}{dt} = \mathbf{\Gamma} - \frac{\mathbf{J}}{t_{gas}}, \tag{39}$$

$$\frac{Jd\cos\gamma}{dt} = -\frac{dJ}{dt}\cos\gamma + \frac{dJ_\parallel}{dt}, \tag{40}$$

where $\mathbf{\Gamma}$ is the RAT, and $J_\parallel = J\cos\gamma$ is the component of angular momentum along the maximal inertia axis.

Assuming that both precession time-scales of $\mathbf{a}_1$ around $\mathbf{J}$ and $\mathbf{J}$ around $\mathbf{B}$ are much smaller than the crossover time, we obtain

$$\frac{dJ}{dt} = M(\langle H\rangle_+ f_+ + \langle H\rangle_- f_-) - \frac{J}{t_{gas}}, \tag{41}$$

$$\frac{d\xi}{dt} = \frac{M}{J}(\langle F\rangle_+ f_+ + \langle F\rangle_+ f_-), \tag{42}$$

$$\frac{J\ d\cos\gamma}{dt} = (\langle Q_{a1}\rangle_+ f_+ - \langle Q_{a1}\rangle_- f_-) - \frac{dJ}{dt}\cos\gamma - (1-\cos\gamma)J, \tag{43}$$

where $M = \frac{\gamma u_{rad} a_{eff}^2 \overline{\lambda}}{2}$, $\langle Q_{a1}\rangle$ is the torque component along the axis $\mathbf{a}_1$, f_+, f_- are probability of finding grains in the positive and negative flipping states, respectively (see WD03).

In equation (43), the component Q_{a1} which is along $\mathbf{a}_1$ also involves the flipping probability because after each flipping, $\gamma \to \pi - \gamma$ for which Q_{a1} changes the sign, i.e., $Q_{a1}(\pi - \gamma) \sim -Q_{a1}(\gamma)$ while equation (43) describes the variation of γ only due to RATs.

7.2 Crossover: no averaging over thermal fluctuations

Let us consider first a grain with $a_{eff} \gg a_c$ for which the crossover time $t_c \ll t_{tf}$. the grain studied is 0.2 micron, and this phrase is not correct. In this case, as the thermal flipping is negligible, the motion of grains comprises the alignment of $\mathbf{J}$ with respect to $\mathbf{B}$ and the motion of $\mathbf{a}_1$ about $\mathbf{J}$. We solve the equations of motion with the initial condition $J_0 = 2J_{th}$ and $\gamma_0 = \pi/4$. Clearly, when the alignment time corresponding to the former case is shorter than the crossover time, then the grains are quickly driven to the attractor points. In particular, grains that become aligned at high J attractor points do not undergo crossovers, but others that are driven to low-J attractor points do. The trivial consequence of this is that, as γ changes, it can alter $\langle F\rangle_\phi$ and $\langle H\rangle_\phi$ because they depend on Θ, which is a function of γ and ξ (see Appendix A).

7.2.1 Only low-J attractor points

If we consider the crossover of a grains (e.g. the *spheroidal* AMO) for the radiation direction $\psi = 30^\circ$ for which only low-J attractor points are present in the phase trajectory map. The grain dynamics of this grain is similar to the case studied in Paper I.

7.2.2 High-J and low-J attractor points coexist

Now let us consider a situation when both high-J and low-J attractor points are present in the phase trajectory map (e.g. $\psi = 0^\circ$ for shape 1). As discussed earlier, irregular grains undergo *irregular* wobbling (cf. thermal wobbling) which induces averaging RATs over three Euler angles. Therefore, the obtained RATs are functions of s (see Fig 22). For simplicity, we assume that the dependence on γ of averaged RATs for irregular grains is similar to that of axisymmetric grains, and thus we can solve equations of motion (41)-(43) for phase trajectories. In fact, the above assumption is feasible when the slightly irregular grains with $I_2 \sim I_3$.

The results for irregular grains are shown in trajectory maps (see Fig. 24). One result that can be seen directly from Fig. 24 is that grains do not reach the low attractor point with $J = 0$ as seen in the phase maps in the absence of thermal fluctuations. Instead, they first tend to reach $J < J_{th}$, and then reverse their direction to head for the high-J attractor point. This stems from the property of RATs. Indeed, the torques are functions of Θ, angle between $\mathbf{a}_1$ and $\mathbf{J}$,$\mathbf{k}$. Therefore, we can qualitatively explain the effect based on the relationship of ξ, Θ and γ. Firstly, for grains with initial angles $\xi < \pi/2, \gamma = 0$, the spinning up torques $H < 0$ and $F > 0$ (see Fig 23). Therefore, the angular momentum of grains decreases while their alignment angle ξ increases. In a short time, γ increases, which gives rise to the change in sign of F and H (see also §6.1). Thus, grains start to reverse their orientation (ξ decreases) and they are spun up to the high-J attractor points. Finally, a perfect alignment at the high attractor point is established.

We see here the difference in the crossover for irregular grains and the *spheroidal* AMO. For example, the difference is evident from the different variation of RATs averaged over free-torque motion for the spheroidal and irregular grains (see Fig. 22). There it is shown that RATs for irregular grains (*ellipsoidal* AMO) change the sign at small deviation angle γ compared to $\gamma = \pi/3$ for the *spheroidal* AMO. It turns out that when grains are driven to low-J attractor points, they can be spun up again as seen in Fig. 24 (cf. Fig. 14).

Fig. 24 (lower panel) represents the phase map for the parallel component $J_\parallel$. It reveals that $J_\parallel$ evolves tightly with J. However, grains undergo multiple crossovers (i.e. $J_\parallel = 0$) before being spun up to high J attractor points. Fig. 24 also indicates that during the crossovers, the angular momentum of grains is about the thermal angular momentum associated with the grain temperature.

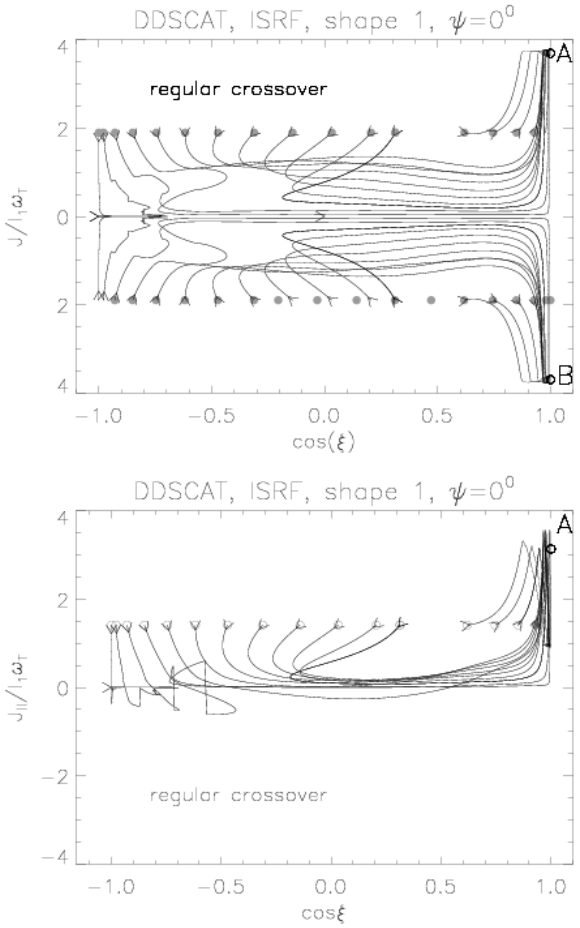


Figure 24. The phase maps for the angular momentum J (*Upper panel*) and the component of $\mathbf{J}$ along the maximal inertia axis $\mathbf{a}_1$ (*Lower panel*). The lower panel shows that grains experience multiple crossovers.

One appealing feature seen in the phase map is that without thermal fluctuations, grains are not trapped at low-J attractor points. They can be spun up after crossovers. However, as thermal fluctuations are considered, the results in §4 and 5 show that grains are still trapped at low-J attractor points.

7.3 Crossover: Averaging over thermal fluctuations

For grains of effective size comparable to the critical size, the thermal fluctuations are important because of the dependence of the Barnett relaxation time on the grain size (see Table 1). In this case, we can consider the grain dynamics in two different regimes. First, assuming that for J greater than J_{th}, the crossover time is shorter than the Barnett relaxation time, then the crossover can be treated as in §7.2. As a result, grains undergo multiple crossovers (see Fig. 25 for the phase trajectories with $J > J_{th}$). As $J \leqslant J_{th}$, thermal fluctuations occur faster than the crossover time, therefore, RATs must be averaged over thermal fluctuations. The dynamics of grains in this stage is the same as studied in §4 and 5 (i.e. grains are trapped at low-J attractor points).

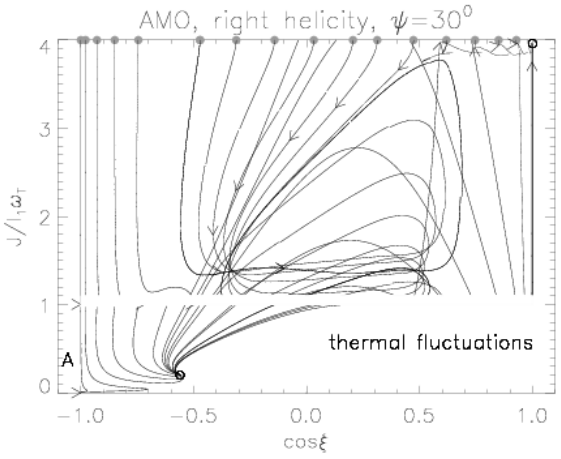


Figure 25. The phase map of grains into different regimes corresponding to the cases with and without thermal fluctuations. For $J > J_{th}$, this figure represents phase trajectories without averaging over thermal fluctuations; grains undergo multiple crossovers. For $J \leqslant J_{th}$, this figure shows the regime in which RATs are averaged over thermal fluctuations; it is shown that grains get aligned at the attractor point A, which is similar to what obtained in §6.

The critical size a_c depends on the radiation energy in the anisotropic flux as $u_{rad}^{-1/2}$. Thus the alignment near stars and in the diffuse ISM is perhaps different.

8 FAST ALIGNMENT

In Paper I we showed that the grains can be aligned over a time scale much smaller than the gas damping time. Now let us consider this problem when thermal wobbling and flipping are important.

Fig. 26 shows the trajectory map constructed from an *ellipsoidal* AMO with $Q_{e1}^{max}/Q_{e2}^{max} = 0.78$ and the light direction $\psi = 70^{\circ}$. The arrow represents a time interval $\Delta t = 10t_{phot}$ where t_{phot} defines the time-scale over which RATs decelerate grains from $J = J_{th}$ to $J = 0$ in the absence of gas damping. It can be seen that the angular momentum of the low attractor point is the same as the case in which the gas damping is included (cf. Fig. 14). We observe that a significant number of grains are aligned on low-J attractor points A, B, C and D over $t_{ali} \sim 40t_{phot}$ (see Fig. 26).

As discussed in Paper I, this type of fast alignment can occur in a diffuse medium with high radiation intensity, such as in the supernovae vicinity or comet wakes. This stems from the fact that strong radiation can drive grains faster to the low- J attractor points where the thermal fluctuations act to maintain the stability of grain alignment.

9 INFLUENCE OF RANDOM BOMBARDMENT BY ATOMIC GAS

In Paper I we showed that in most cases RATs align grains with respect to magnetic fields while decreasing the grains's angular momentum to $J = 0$. The results above indicate that thermal fluctuations can change a zero-J attractor point to a $J \sim J_{th}$ attractor point. In addition, atomic collisions can affect the alignment established by RATs in the

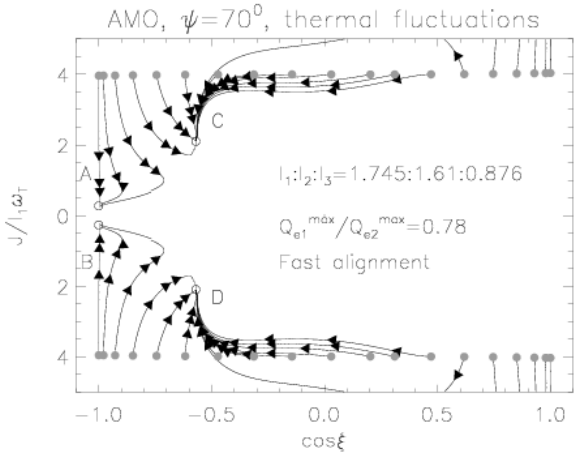


Figure 26. Similar to Fig. 14 but the gas damping is neglected. The arrow represents a time interval $10t_{phot}$.

presence of thermal fluctuations. In this section, we first briefly discuss the method of studying gas bombardment based on the Langevin equation. Then, we show the influence of this process on RAT alignment.

9.1 Method

The effects of collisions in the framework of paramagnetic alignment have been studied by many authors (Jones & Spitzer 1967; Purcell 1971; Purcell & Spitzer 1971; Lazarian 1997) using the Fokker-Planck equations. However, the Langevin approach was used to study this problem numerically in Roberge, Degraff & Flatherty (1993) and Roberge & Lazarian (1999). The afore-cited papers used the equivalence of the Fokker-Planck and the Langevin equations to simulate the evolution of angular momentum of grains in a gas coordinate system. They derived explicit diffusion coefficients for random torques acting on spheroidal grains. According to the above works, an increment of angular momentum resulting from gas-grain collisions within an infinitesimal time interval dt is (see Roberge et al. 1993)

$$dJ_i = A_i(t)dt + B_{ij}(J,t)dw_j,\ i = x,y,z, \tag{44}$$

where $d\omega_j$ are Wiener coefficients, A_i, B_{ij} are diffusion coefficients, given by

$$A_i = \langle \Delta J_i \rangle,\ i = x,y,z, \tag{45}$$

$$(BB^T)_{ij} = \langle \Delta J_i \Delta J_j \rangle, i,j = x,y,z, \tag{46}$$

where B^T is the transposal matrix of $\mathbf{B}$. Similar to Roberge et al. (1993), diffusion coefficients are first calculated in the grain body frame, and then transformed to the lab system. The diffusion coefficients are averaged over the precession of $\hat{\mathbf{a}}_1$ around $\mathbf{J}$ and over the Larmor precession angle of $\mathbf{J}$ about $\mathbf{B}$, given by

$$\langle \Delta J \rangle_i = -\frac{J_i}{t_{gas}}, \tag{47}$$

where t_{gas} is the gaseous damping time. For a spheroidal grain, the gaseous damping time is

$$t_{gas} = \frac{3}{4\sqrt{\pi}} \frac{I^b_{zz}}{nmv_{th}b_m^4 \Gamma_{\parallel}(e_m)}, \tag{48}$$

where I^b_{zz} is the moment of inertia of the grain along zz axis (i.e., along the maximal inertia axis $\hat{\mathbf{a}}_1$), $v_{th} = \sqrt{2mkT_{gas}}$ is the thermal velocity of atom, and b_m is the semi-axis of the grain. $\Gamma_{\parallel}, \Gamma_{\perp}$ are factors characterizing the geometry of grain given by

$$\Gamma_{\parallel} = \frac{3}{16}3 + 4(1-e_m^2)g(e_m) - e_m^{-2}[1-(1-e_m^2)^2 g(e_m)], \tag{49}$$

$$\Gamma_{\perp} = \frac{3}{32}[[7 - e_m^2 + (1-e_m^2)g(e_m) + (1-2e_m^{-2}) (1+e_m^{-2})^2[1-(1-e_m^2)g(e_m)]]]. \tag{50}$$

$g(e_m)$ is related to the eccentricity of the grain through the expression:

$$g(e_m) = \frac{1}{2e_m}\ln(\frac{1+e_m}{1-e_m}), \tag{51}$$

where $e_m = \sqrt{1-(a/b)^2}$. Diffusion coefficients are diagonal and given by the following expressions in the lab coordinate system in which the z axis is along the magnetic field (Roberge et al. 1993)

$$\langle (\Delta J_x)^2 \rangle = \frac{\sqrt{\pi}}{3} nm^2 b_m^4 v_{th}^3 (1 + \frac{T_d}{T_g}) \times [(1+\cos^2\xi)\Gamma_{\perp} + \sin^2\xi\Gamma_{\parallel}], \tag{52}$$

$$\langle (\Delta J_y)^2 \rangle = \langle (\Delta J_x)^2 \rangle, \tag{53}$$

$$\langle (\Delta J_z)^2 \rangle = \frac{2\sqrt{\pi}}{3} nm^2 b_m^4 v_{th}^3 (1 + \frac{T_d}{T_g}) \times [\sin^2\xi\Gamma_{\perp} + \cos^2\xi\Gamma_{\parallel}]. \tag{54}$$

Note that the above diffusion coefficients are derived by assuming perfect internal alignment of $\mathbf{a}_1$ with $\mathbf{J}$ and for spheroidal grains. However, for the sake of simplicity, we can adopt these diffusion coefficients for studying the influence of gas bombardment on the alignment of irregular grains.

9.2 Results

First, we solve the Langevin equation (i.e. equation 44) for grains subjected to random torques as a result of gas collisions, assuming that the diffusion coefficients remain the same for irregular grains. We use the initial condition $J = J_{th,gas} = \sqrt{2I_1 kT_{gas}}$, ξ is generated from a uniform distribution in the range 0 to π and ϕ is a free parameter. Wiener coefficients $d\omega$ in equation (44) are generated from a Gaussian distribution function at each time-step. Then the resulting solution J_x, J_y and J_z are taken as input parameters for solving the equations of motion of grains driven by RATs in the spherical coordinate system described by J, ξ, ϕ (see equations (15)-(17)) to obtain new values of J and ξ.[11] This process is performed over $N = 10^6$ time-step $\Delta t = 10^{-4} t_{gas}$. Other physical parameters for the ISM are taken from Table 1. The alignment angle ξ is used in averaging over the total time to obtain the degree of external alignment, and J is used to calculate the internal alignment, assuming that thermal fluctuations follow a Gaussian distribution.

For the AMO, we consider our default model of $\alpha = 45^\circ$

[11] Here we average over the Larmor precession angle ϕ.

(see Paper I). For DDSCAT, we study the entire spectrum of the ISM for grain shapes 1 and 3 with size $a_{eff} = 0.2\mu m$.

9.2.1 Influence of randomization to the phase trajectory map in the presence of high−J attractor point

We can see that collisions have an interesting effect on grain dynamics when the high attractor point is present. Random collisions are very efficient for low-J. So, the motion of grains is disturbed by random collisions when they approach the low-J attractor point. After a time interval, grains enter the region of $\cos\xi > 0$ (i.e., positive spinning radiative torque) for which RATs can spin up to the high J attractor point. Therefore, for this case, random collisions *increase the degree of alignment*. The percentage of grains present in the vicinity of the high-J attractor points as a function of time is shown in the upper panel in Fig. 27. The respective degree of alignment is shown in the lower panel.

From the upper panel (Fig. 27), we find that, during the time interval $t = t_{gas}$, only about 10% of grains are present at the high $-J$ point. Then it increases with time and attain the saturated value of 75% after $t = 40t_{gas}$.

Following the lower panel in Fig. 27, we see the rise of the degree of alignment with time. It get to a significant value after $t = 10t_{gas}$, and the alignment is nearly perfect with $R = 0.8$ after $t = 80t_{gas}$.

Due to the stochastic properties of gas bombardment, the degree of alignment depends on the angular momentum of the high attractor point $J_{high}(\psi)$. A detailed study of the degree of alignment with $J_{high}(\psi)$ in Hoang & Lazarian (; in preparation) shows that the alignment at high attractor points is nearly perfect if $J_{high}(\psi) \geqslant 3J_{th,gas}$ where $J_{th,gas}$ is the angular momentum corresponding to the temperature of the ambient gas.

9.2.2 Influence of randomization to the phase trajectory map in absence of high-J attractor point

The degree of alignment for the *spheroidal* AMO and irregular grains in the absence of high-J attractor points is shown in Fig. 28. For these cases, random collisions act to decrease the alignment. This arises from the fact that random collisions remove grains from the low-J attractor points. We have found that if the angular momentum of the high-J stationary point, $J_{high}(\psi)$, larger than $J_{th,gas}$, RATs move grains to the vicinity of the high-J stationary points, and decelerate them again. It is seen that although R is decreased by gas bombardment, it is still not negligible (e.g., about 0.1 and 0.2 for AMO and irregular grains; see Fig. 28).

For $J_{high}(\psi) < J_{th,gas}$, grains are in a fully thermal regime. Therefore, the phase map of grains is mostly random. From the lower panel in Fig. 28, it follows that the degree of alignment is marginal. However, a more elaborate treatment in Hoang & Lazarian (in preparatiom) does not use equation (2) and demonstrate higher degree of alignment.

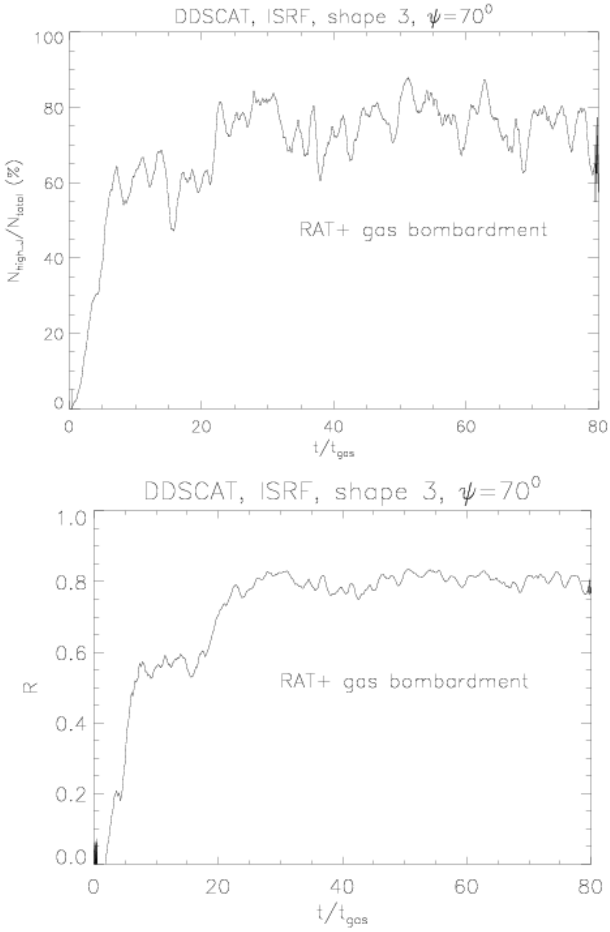


Figure 27. For the ISRF, shape 3, and $\psi = 70°$:*Upper panel* shows the variation of the percent of grains present in the vicinity of the high J attractor point A, B in time, and *lower panel* shows the Rayleigh reduction factor for this case.

10 INFLUENCE OF H_2 FORMATION TORQUES ON GRAIN ALIGNMENT

When a hydrogen atom sticks to a grain, it starts its diffusion over the grain surface. In general, the grain surface is never uniform, and there are always certain special catalytic sites where hydrogen atoms can be trapped (see Purcell 1979; Lazarian 1995). A wandering H atom on the grain surface may encounter another atom dwelling at the catalytic site and a reaction takes place, producing a H_2 molecule. The ejected H_2 molecule acts as miniature rocket thrusters. Averaging over the grain surface (e.g. a brick surface), H_2 rockets produce a net angular torque that is parallel to the maximal inertia axis (Purcell 1979). However, resurfacing or poisoning by accretion of heavy elements can destroy the catalytic sites and create new ones. As a result, H_2 torques change both magnitude and direction over a definite time scale t_L, so-called resurfacing time.

10.1 Method

Purcell (1979) used the Monte Carlo method to simulate the variation of the torque as a result of grain resurfacing. Roberge & Ford (2000) used the equivalence of the Langevin

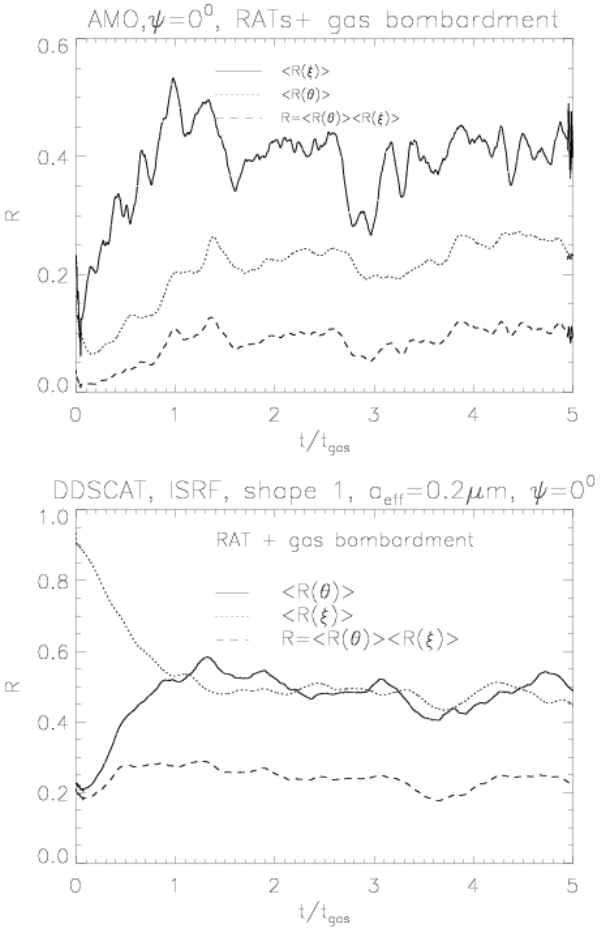


Figure 28. Figs show dynamics of external, internal degree of alignment and Rayleigh reduction factor in time corresponding to RATs from the AMO (*upper panel*) and DDSCAT (*lower panel*) when the phase trajectory maps do not have high-J attractor points.

and the Fokker-Plank equations to simulate the H_2 torque. They model L_z as a Gaussian process that is averaged to zero in time, and the correlation function that is exponential:

$$\overline{L_z^b(t)} = 0, \tag{55}$$

$$\overline{L_z^b(t)L_z^b(t-\tau)} = \langle(\Delta L_z)^2\rangle \exp(-\tau/t_L). \tag{56}$$

In equation (56), $\langle(\Delta L_z)^2\rangle$ is the magnitude of H_2 torque given by

$$\langle(\Delta L_z)^2\rangle^{1/2} = \frac{1}{3}(\frac{\pi}{3})^{1/6} f n(H)(2EkT_{gas})^{1/2} a_{eff}^2 l, \tag{57}$$

where f is the fraction of H atoms absorbed by the grain and converted to H_2, $n(H)$ is the H density, E is the kinetic energy of each departing H_2 and l is the side of the individual catalytic site (Purcell 1979; Lazarian & Draine 1997).

In an interval of time dt, the torque along the axis $\mathbf{a}_1$, L_z^b , can be simulated by a Gaussian process with the correlation time scale t_L, given by the Langevin equation (Roberge & Lazarian 1999)

$$dL_z^b = -L_z^b \frac{dt}{t_L} + [2\frac{\langle(\Delta L_z)^2\rangle}{t_L}]^{1/2} dw, \tag{58}$$

where dw is a random variable, independent of time, sampled from a Gaussian distribution function, and $L_z^b(t)$ is the instant torque at time t. This equation allows us to follow the evolution of H_2 torque in time.

When the internal relaxations (Purcell 1979; Lazarian & Draine 1999b) are taken into account, the angle γ between the maximal inertia axis $\mathbf{a}_1$ and the angular momentum fluctuates in time. However, as the fluctuation timescale is much shorter than the alignment time-scale, we do not follow the evolution of this angle. Instead, we average over this. Following Spitzer & McGlynn (1979), the mean H_2 torque for a spheroid is given by

$$\mathbf{\Gamma_{H_2}} = L_z^b \overline{\cos\gamma} \frac{\mathbf{J}}{J}, \tag{59}$$

where $\overline{\cos\gamma}$ denotes the average of $\cos\gamma$ over thermal fluctuations as defined by equation (12), which defines the value of the projection of $\mathbf{L}_z^b$ onto the angular momentum axis $\mathbf{J}\|\hat{Z}$. For irregular grains, $\overline{\cos\gamma}$ in equation (59) is replaced by the thermal average, $\overline{C}$, of C which is given by

$$C = (\frac{I_1 - I_3 q}{I_1 - I_3})^{1/2} \frac{\pi}{2F(\pi/2, k^2)} \text{ for } q < \frac{I_1}{I_2}, \tag{60}$$

and

$$C = (\frac{I_3(q-1)}{I_1 - I_3})^{1/2} \frac{\pi}{2F(\pi/2, k^{-2})}, \text{ for } q > \frac{I_1}{I_2}, \tag{61}$$

where k^2 and F are given in Appendix C (see WD03).

Because of the grain flipping, equation (59) becomes

$$\Gamma_{H2}^J = L_z^b \overline{\cos\gamma}(f_+ - f_-). \tag{62}$$

where f_+ and f_- are probability of finding the grain in positive and negative flipping states, respectively.

The equations of motion (i.e. equations 16-17) of grains by RATs and H_2 torque read

$$\frac{d\xi}{dt} = \frac{\gamma u_{\rm rad} a_{\rm eff}^2 \overline{\lambda}}{2J} \langle F(\xi,\phi,\psi,J)\rangle_\phi, \tag{63}$$

$$\frac{dJ}{dt} = \frac{1}{2}\gamma u_{\rm rad} a_{\rm eff}^2 \overline{\lambda} \langle H(\xi,\phi,\psi,J)\rangle_\phi - \frac{J}{t_{gas}} + \Gamma_{H_2}^J, \tag{64}$$

where we have averaged RAT components over the Larmor precession angle ϕ.

10.2 Results

We solve the equations of motion for grains subjected to RATs and H_2 torques using the Runge-Kutta method with a finite time-step, $\Delta t = 10^{-4} t_{gas}$ and $N = 10^5$ time-steps . We use the initial condition $J = 20 J_{th}$, and ξ is generated from a uniform angle distribution in the range from 0 to pi. At each time-step, we first solve the Langevin equation (equation 58) for components of H_2 torques. Then, by subsituting the resulting H_2 torques into equations 63)-(64), we solve the obtained equations for J and ξ. The resulting solutions J and ξ are used to construct trajectory maps and calculate the degree of alignment.

10.2.1 Trajectory maps

Fig. 29 shows the map when the variation of H_2 torques is accounted for (lower panel), compared with the map driven by RATs (upper panel) produced by a radiation field of

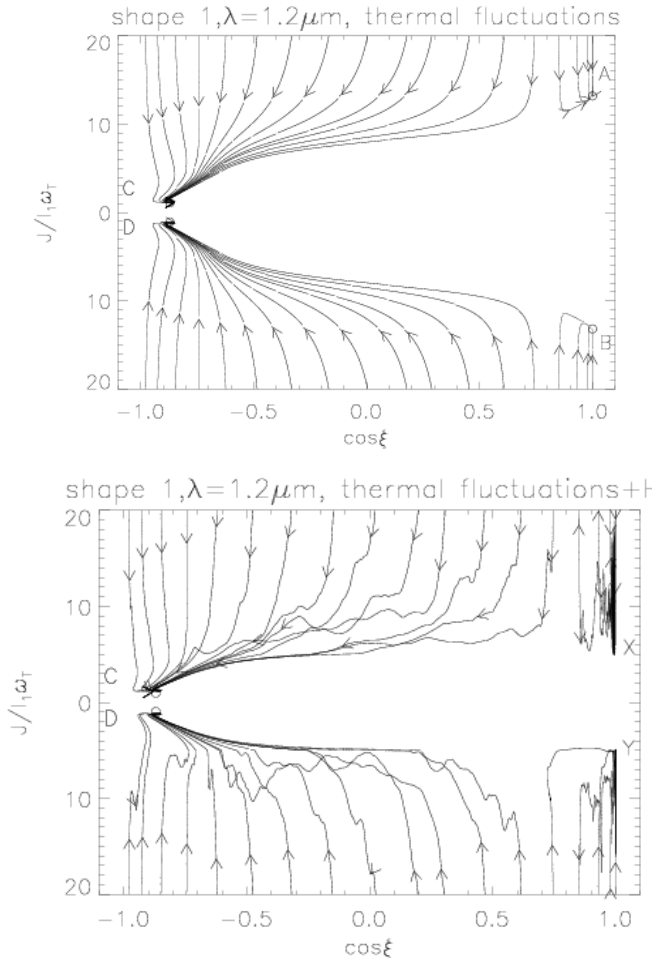


Figure 29. *Upper panel:* map trajectory of grain $a_{eff} = 0.2\mu m$ and $\lambda = 1.2\mu m$ by RATs; *lower panel:* when H_2 torque varies due to resurfacing of active sites on grains surface. The results show that, during the spin-down, grains are driven by RATs to thermal angular momentum. However, because grains flip very fast, H_2 torques become inefficient to spin up grains at low-J attractor points.

$\lambda = 1.2\mu m$ for a grain with size $a_{eff} = 0.2\mu m$. We assume that the resurfacing process on the grain surface occurs rapidly, so we model the variation of H_2 torques with the correlation time-scale $t_L = 0.1t_{gas}$. In the absence of H_2 formation torques, RATs drive grains to attractor points. A significant fraction of grains are driven to low attractor points marked by C, D, at $J/I_1\omega_T \sim 1$, and some grains are aligned at attractor points A, B corresponding to high angular momentum (see the lower panel in Fig. 29).

Consider now a case of when H_2 torque amplitude is larger than that of RATs (e.g. consider the radiation direction $\psi = 70°$). It is obvious that RATs still dominate the Purcell torque for this case, and drive a significant number of grains to the low attractor points C and D. In fact, at the initial phase of $J \gg J_{th}$, grains are spun up by the Purcell torque; however, during the spin-down, RATs lead grains to low-J attractor points. Because of grains having low angular momentum at the low-J attractor points, grains flip fast and the Purcell torques are averaged to zero (see the lower panel in Fig. 29) similar to what is described in Lazarian & Draine (1999a). Therefore, the trajectory map with two attractor points C, D of low angular momentum is determined by RATs as in the case without H_2 torques (see the upper panel in Fig. 29). However, for the attractor points A, B with high angular momenta, the thermal flipping does not occurs because of $J \gg J_{th}$. In other words, during spin-down period, grains are driven by H_2 torques to reach the low angular velocity regime. As J decreases, RATs become dominant and drive grains to attractor points C, D, as shown in the lower panel of Fig. 29. However, as J increases, H_2 formation torques become dominant and do not allow grains to have attractor points. Therefore, attractor points A, B become unstable, and grains are spin up and down by H_2 torques and RATs in the range between X and Y (see the lower panel in Fig. 29), corresponding to $J/J_{th} = 5$ to 40. The range of such a variation depends on the relative amplitude of H_2.

When the correlation time-scale $t_L = 10t_{gas}$, our results show that trajectories of grains ending at high-J attractor points C, D are marginally affected by H_2 torques, because RATs eventually drive grains to these attractor points at which the fast thermal flipping destroys completely the influence of H_2 torques. In contrast, grains that are driven to X and Y experience the same effect as in the case $t_L = 0.1t_{gas}$.

For $t_L \to \infty$, H_2 torques act to spin grains up. Therefore, the low-J attractor points become high -J attractor points, provided that H_2 torques dominate RATs.

For larger grains, thermal flipping is less important (see Lazarian & Draine 1999a) , so H_2 torques are important even during the slow rotation period, influencing significantly the radiative alignment. We provide the treatment of this case elsewhere.

10.2.2 Dynamics of degree of grain alignment

Fig. 30 shows the variation of the degree of alignment $\langle R\rangle$ in time for the cases in which only RATs are considered (upper panel) and RATs plus H_2 torques with the correlation time-scale $t_L = 0.1t_{gas}$ are taken into account (lower panel).

It is seen from Fig. 30 that the degree of alignment $\langle R\rangle$ is the same for the case $\psi = 70^0$ because of the dominance of RATs in driving grains to attractor points. At $\psi = 30^0$, the alignment degree exhibits small variations. In addition, for both directions, $\langle R\rangle$ does not increases smoothly to a stable value as in the case of alignment by only RATs as grain dynamics is affected by the stochastic variation of H_2 torques. When grains are driven to the attractor points with thermal angular momentum A and B, the fast thermal flipping of grain wipes out the effect of H_2 torques, which are fixed in the grain body coordinate system. Therefore, the grain alignment is mostly determined by RATs.

10.3 Alignment by RATs, H_2 formation torques and gas bombardment

In most cases, RATs play the key role in aligning grains with a magnetic field, while H_2 is only important to spin up grains. Moreover, for grains smaller than $\sim 10^{-4}$cm, thermal flipping is very fast, and thus the influence of H_2 torques is rather marginal. In contrast, for large grains $\geqslant 10^{-4}$ cm, H_2 torques could be significant for the grain alignment . On the

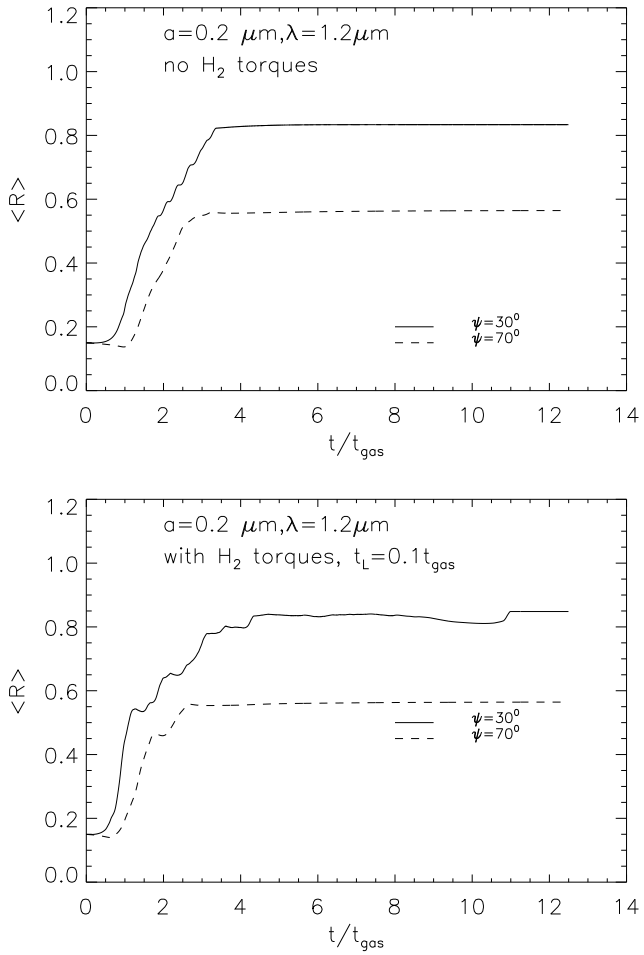


Figure 30. Panels show the variation of degree of alignment $\langle R\rangle$, of **J** with **B** in time for the monochromatic light illuminating grain in two directions $\psi = 30°$ and $70°$. *upper panel:* only RATs align grains and they have stable orientation; *lower panel:* the same as the lower panel, but H_2 torques with a correlation time-scale $t_L = 0.1t_{gas}$ are included.

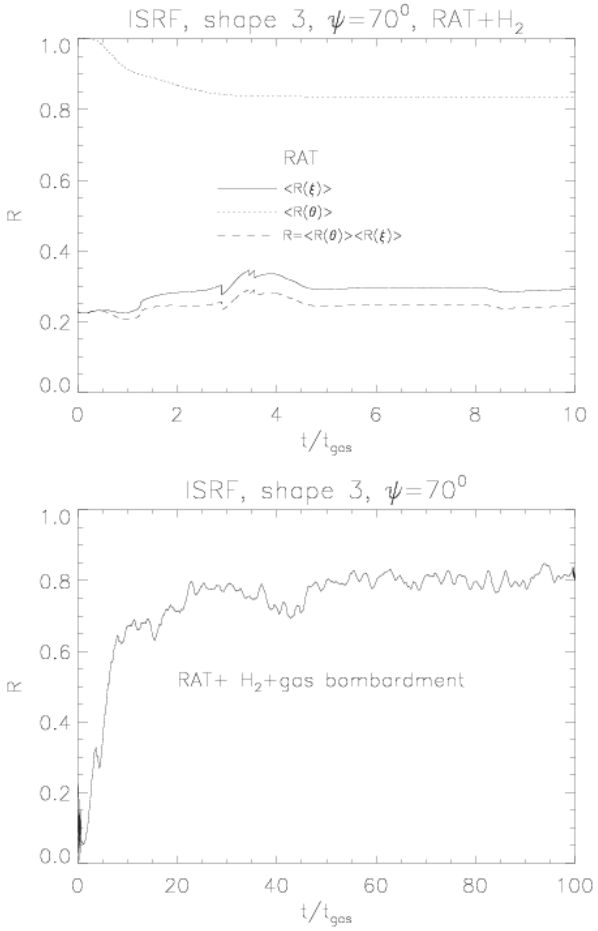


Figure 31. The Rayleigh reduction factor for grain $a_{eff} = 0.2\mu m$ aligned by RATs, H_2 formation torques (*upper panel*) and by RATs, H_2 and gas bombardment (*lower panel*).

other hand, random collisions affect the alignment of grains mostly when grains rotate at thermal velocity. The upper panel in Fig. 31 shows both internal and external degree of alignment as well as the Rayleigh reduction factor for the alignment induced by RATs and H_2 torques. It is seen that $R \sim 0.25$ for this case. However, when gas bombardment is taken into account, we found that R increases to $R = 0.75$ (see the lower panel in Fig. 31). In fact, this increase is not unexpected, since for this case, grains are driven by gas bombardment to high attractor point, which increases the degree of alignment as discussed in §8.

11 DISCUSSION

11.1 Central role of the AMO

Our understanding of the RAT alignment has been improved considerably when a simple model of a helical grain (i.e. the AMO), was introduced in Paper I. With the assumption of perfect internal alignment, the AMO reproduced the alignment effects similar to irregular grains studied by DDSCAT (see Paper I). For instance, the AMO shows that for a given shape, size and radiation field, some grains can be spun up to suprathermal rotation and aligned at high-J attractor points, while most of grains are driven to low-J attractor points. Moreover, the AMO demonstrated that whether RATs can spin-up grains to high J attractor points depends on the ratio of the torque components Q_{e1} and Q_{e2}.

The correspondence of the AMO to DDSCAT calculations of RATs for irregular grains in Paper I encouraged us to use the AMO for the case when thermal wobbling is taken into account. In our study, we used the AMO assuming that its inertial properties are defined by a triaxial ellipsoid rather than a spheroid. This was very easy to accomplish, as, within the AMO, torques acting upon either spheroidal, or ellipsoidal body induce only precession, while the actually important torques (i.e. Q_{e1} and Q_{e2}) arise from the mirror. We found a number of differences in the AMO dynamics for the two cases. We treat the AMO with ellipsoid of inertia as our generic case.

11.2 Treatment of free wobbling

In Paper I we showed that Q_{e3} in the AMO can be negligible when considering the alignment and spin-up torques. We have found again that the component Q_{e3} for the AMO also plays a marginal role in alignment, as well as, spinning up grains if we followed the algorithm in WD03 and averaged RATs over a sufficient time-steps (e.g. about $N = 10^3$; see §3.3). Using our new algorithm of averaging in which we solve the differential equation for the rotation angle ζ instead of assuming that this angle ranges from 0 to 2π, we obtained similar results when the averaging is perfomed over a much longer time (e.g. $P = 10^3 P_\tau$). It contributes mainly to the precession about the radiation beam axis **k** (see Fig. 1). As a result, in most practical situations, it is sufficient to deal with only two RAT components Q_{e1} and Q_{e2}.

We studied the alignment for two cases (1) when thermal relaxation time-scale is much shorter than the crossover time (i.e., averaging RATs over thermal fluctuations) and (2) when the thermal relaxation time scale is much longer than the crossover time. For the former case, grains are directly aligned at low-J attractor points. In contrast, the grains undergo multiple crossovers in the second case.

The AMO enables us to average RATs analytically over thermal fluctuations assuming a Gaussian distribution. The obtained expressions allowed us to gain important insights into the role of thermal wobbling.

11.3 Direction of grain alignment

It has been shown in Paper I that the alignment by RATs occurs mainly with the longer axis perpendicular to the magnetic field. However, there was still a narrow range of radiation directions for which grains were aligned with longer axes parallel to magnetic field (i.e. "wrong" alignment). We have shown that the "wrong" alignment can no longer exist because of the fast wobbling of the grains. Indeed, in Paper I we found that "wrong" alignment takes place for a low-J attractor point for a narrow range of angles around the angle between the light direction and magnetic field $\psi = \pi/2$. This range is narrower than the range of grain wobbling at the low-J attractor point. The disappearance of the "wrong" alignment was, in fact, predicted in Paper I. A direct implication this effect is that allows a more reliable interpretation of the observation data: grains are aligned with long axes perpendicular to magnetic field when they are aligned by RATs.

11.4 Degree of grain alignment and critical size

The degree of external alignment of angular momentum with the magnetic field can achieve unity. However, because of the weak coupling of the maximal inertia axis of grain with the angular momentum at low-J attractor points, the Rayleigh reduction factor R is lower than unity. A new effect that we discuss in this paper is the transition of grains from low-J to high-J attractor points, in situations when such attractor points coexist. This increases the degree of alignment. Interestingly enough, the transition which makes grains better aligned is induced by *random bombardment* (see §9).

The degree of alignment depends on the angular momentum J_{high} of the high attractor points. The value of J_{high} is a function of RATs that increases with grain size. Because of the gas bombardment, only grains aligned with $J_{high} > J_{th}$ can maintain the stable alignment with the magnetic field. The minimal size corresponding to $J_{high,min}$ is named the critical size. For the irregular shape 1 and the ISRF, by studying the alignment for grains with size spanning from $0.025\mu m$ to $0.2\mu m$, we found that the critical size of aligned grains is about $0.05\mu m$, assuming that $J_{high,min} = 3J_{th}$. Apparently, critical size depends on radiation field. Therefore, for attenuated field, e.g. dark molecular clouds, the critical size is shifted to larger value (i.e., only large grains can be aligned by RATs).

11.5 Role of paramagnetic dissipation

Paramagnetic dissipation does not play any role in the RAT alignment. Although the predictions of RAT alignment coincides with the predictions by the Davis-Greenstein mechanism (i.e. the alignment with long axes perpendicular to the magnetic field), RAT alignment occurs over shorter time scale compared to paramagnetic relaxation time t_{DG}, provided that grains are paramagnetic.

As a result, unless grains are superparamagnetic (see Jones & Spitzer 1967; Mathis 1986), paramagnetic relaxation is irrelevant. A common fallacy entranced in the literature is that RAT alignment is a sort of paramagnetic alignment of suprathermally rotating grains, i.e. kind of alignment of fast rotating suggested by Purcell (1979), but with fast alignment produced by RATs. This way of thinking of RAT alignment is erroneous, as, unlike the Purcell (1979) torques, RATs induce their own alignment, which is faster than the paramagnetic one.

11.6 Effects of radiation field intensity

When grains are aligned at high-J attractor points, the variations of radiation intensity induce the variation in J value. However, a significant fraction of grains that align at low -J attractor points at which J does not vary with radiation intensity. Therefore, after a certain threshold at which grains are aligned suprathermally (i.e. with $\omega \gg \omega_{thermal}$) at high-$J$ attractor point the increase of radiation intensity does not increase the degree of alignment for grains aligned at such points.

When grains are aligned at low-J attractor points, a weaker alignment is expected, because of the poor coupling of the maximal inertia axis with angular momentum for low J (see Lazarian 1994; Lazarian & Roberge 1997), irrespective of the intensity of radiation field. The increase of the radiation intensity does not affect the position of lower-J attractor points.

11.7 Role of gas bombardment and H_2 torques

This is the first study to take into account the effects of gaseous bombardment and H_2 formation within the RAT alignment mechanism. Random gas bombardment itself has always been considered as the cause of grain randomization. However, in the framework of the RAT alignment, its effect can be different.

As discussed in the paper, RATs align grains with respect to the magnetic field while driving grains to high-J and low-J attractor points. Naturally, the later case is more sensitive to gas bombardment. This random process can increase the alignment degree by driving grains from the low-J attractor points to high J attractor points. Such a process gives rise to the time-dependent alignment. The time over which the alignment can become stable is about $10^2 t_{gas}$. For high-J attractor points, the alignment is marginally affected by the bombardment.

H_2 torques were believed to play a major role on the grain alignment. However, we found in the present study that H_2 torques are indeed important for high attractor points for which they can spin grains up. For low attractor points with low angular momentum, the fast flipping of grain axis as a result of thermal fluctuations averages out any torques which are fixed in the grain body, e.g. H_2 torques.

11.8 Time-scales of alignment

If paramagnetic dissipation is neglected, one may guess that the only characteristic time that can determine RAT alignment could be t_{gas} (see DW97). As pointed out in Paper I, strong radiation field can provide grain alignment over a time-scale shorter than the gas damping time (i.e. fast alignment). The characteristic time of this alignment can be $\sim 30 t_{phot}$, where t_{phot} is the time over which the amplitude value of radiative torques can deposit a grain with the angular momentum of the order of its initial angular momentum. The large coefficient in front of t_{phot} reflects relative inefficiency of radiative torques in the vicinity of low-J attractor points. The supernova shell or star forming regions are favorable medium for such a fast alignment.

Our present study shows that another time scale is appropriate, when the phase trajectory map contains both low-J and high-J attractor points. This time is about $\sim 30 t_{gas}$ and it corresponds to the time scale over which the gaseous bombardment transfers grains from low-J to high-J attractor points.

11.9 Role of initial J

The role of initial J for alignment has been studied in Paper I, where we found that it determines the time of "fast" alignment t_{phot}. In addition, in the paper above, we have seen new low-J attractor points present in the phase maps when thermal fluctuations are accounted for. However, if grains start from small J, the grain trajectories may not enter the parameter space, that would induce directing grains to high-J attractor points. Instead, the trajectories may, in the absence of gaseous bombardment, end up at the low-J attractor points.

However, in practical terms, this particular difference is not crucial for the overall dynamics. In the presence of gaseous bombardment, the grains will be moved to the high attractor points, if such points exist.

11.10 Grain dynamics at $J \sim J_{th}$

In Paper I, with the assumption of simplified dynamics, i.e., assuming that $\mathbf{J}$ is always aligned with the maximal inertia axis $\mathbf{a}_1$, we showed that AMO induces a good alignment with respect to radiation direction or magnetic field. The assumption of $\mathbf{J}$ and $\hat{\mathbf{a}}_1$ coupling is correct only for $J \gg J_{th}$. In this paper, we use the analytical formulae for RATs and get the analytical expressions for torques components when thermal fluctuations are accounted for, and therefore the angle between $\mathbf{J}$ and $\hat{\mathbf{a}}_1$ fluctuates. Results show that torque components decrease substantially as thermal fluctuations become stronger (see Figs 7), but the dynamics of grains does not change radically. This interesting finding testifies that thermal fluctuations as a result of internal relaxations do not play the key role in creating the low-J attractor points as it was believed earlier, but they "lift up" the earlier existing attractor points.

In order to see whether the irregularity of grain shape is important, we modify slightly AMO by replacing the spheroidal body by the ellipsoidal one. As earlier discussed, the ellipsoidal body does not affect on Q_{e1}, Q_{e2} for AMO, but changes the dynamics of fluctuations and therefore the averaging. As a result, the torques resulting from averaging over thermal wobbling are different, which induces the difference in the dynamics for irregular grains. Thus, the irregularity of shape and the presence of thermal fluctuations act together when grain angular momentum is comparable with J_{th}.

11.11 Crossovers

We studied the crossover by following the variations of angular momentum and the component parallel to the axis of major inertia in the case when thermal fluctuations are negligible. Our detailed treatment of crossovers is in agreement with the earlier studies by Spitzer & McGlynn (1979) and Lazarian & Draine (1997), but is different from the treatment of crossovers in DW97.

Whereas in Paper I we followed the regular phase trajectories of grains approaching to the crossover, in the present study we take into account thermal wobbling that becomes important as the grain angular momentum becomes comparable with the thermal one. Unlike the approach in WD03, which is applicable only to small grains, our treatment is also applicable to large grains for which initially the time of thermal wobbling (which is of the order of the internal relaxation time) is longer than that of crossovers. We find that both large and small grains eventually get to a similar state, at which the amplitude of the angular momentum gets of the order of its *thermal* value. This corresponds to low-J attractor point.

Our work confirms the claim in Paper I that the low-J attractor points are not metamorphosis of crossover points after which grains spin up again as in DW97 (see also WD03), but a modification of zero-J attractor points, that exists in the absence of thermal fluctuations.

11.12 Helicity of grains

Helicity of grains as a factor of RAT processes was first mentioned in Dolginov & Mytrophanov (1976). However, there it

was not identified what can make grains helical. Moreover, it was claimed that some regions of space can have non-helical grains, which implied that helicity of grains is something that requires rather special conditions to emerge[12] . Later the RAT action was demonstrated for rather arbitrarily shaped grains in DW96, but this and subsequent studies, namely, DW97, WD03, did not use the concept of helicity.

Grain helicity, as an essential requirement for alignment was identified in Paper I, where by comparing results of numerical calculations for irregular grains with AMO, it was established that grains can be classified as either of left or right helicity. Moreover, it was shown that irregular grains demonstrate helicity and, therefore, alignment, not only subject to radiation, but also to gaseous flows (see more in Lazarian & Hoang 2007b).

In Paper I, an irregular grain rotating about its axis corresponding to the maximal inertia axis was identified as a helical grain. Our present study demonstrates the advantage of good internal relaxation of the maximal inertia axis and angular momentum. Indeed, we show that torques acting on a grain decrease when the grain starts wobbling.

11.13 Irregularity of shape and inertia

Irregular grains, in general, have an irregular shape and have to be characterized by a triaxial ellipsoid of inertia, rather than a spheroid. The irregularity of grain shape gives rise to grain helicity, while the irregularity in terms of the moment of inertia modifies grain dynamics. One of the interesting effects that we observed for grains, which can be characterized by a spheroid of inertia, is a transfer of grains from low-J attractor point (actually, zero-J attractor point) to high-J attractor point in the absence of gaseous bombardment. This effect disappears when thermal fluctuations are accounted for.

11.14 Comparison with earlier studies

The irregular torques arising from emission and absorption photons randomly depositing angular momentum to grains were discussed in Harwit (1970). The marginal importance of the mechanism for the alignment was shown, however, in Purcell & Spitzer (1971). Dolginov (1972) proposed the first model of RATs that act on chiral, e.g. quartz, grains. Later, Dolginov & Mytrophanov (1976) considered a more generic case of RATs, i.e. RATs arising from "twisted", irregular grains. The idea of RAT alignment was mostly ignored by the community (see Lazarian 1995, as an exception) until numerical calculations of RATs got available in DW96, DW97. From the earlier studies, the most relevant to this work is WD03, where effects of thermal fluctuations within the RAT alignment were empirically studied.

This work extends our study in Paper I, which demonstrated the ability of the AMO to represent helical grains. The AMO allowed us to address the generic features of the RAT alignment. We note that our procedures of torque averaging and our results for angular momentum for low-J attractor points differ from those in WD03. Our interpretation of the origin of those points is also different.

Extending AMO, we have proven that thermal trapping of grains at the low J attractor points reported in WD03 is generic, i.e. does not depend on the particular direction between the beam and the magnetic field, or on the particular choice of the irregular grain or on the particular wavelength/radiation spectrum chosen. Moreover, we have shown that the we expect the new low J attractor points to appear close to $\cos\xi = 1$, which makes grains aligned with $\mathbf{B}$ at these new attractor points. All the results we obtained with AMO were also tested with two irregular grain shapes. In addition, we accounted for gaseous bombardment and H_2 formation.

11.15 Accomplishments and limitations of the present study

The study above clarified a number of outstanding issues in RAT alignment theory. It relied on the guidance of the analytical studies of RATs and crossovers in Paper I and accounted or the proper averaging of RATs arising from thermal wobbling. It confirmed the predicted in Paper I the gradual change of the position of lower attractor points on the trajectory maps of irregular grains from zero to the thermal value of angular momentum. In addition, our study accounted for the effects of gaseous bombardment and H_2 formation on the RATs. This resulted in a discovery of a new important effect, namely, the transfer of grains from lower attractor points to high attractor points, when the latter points exist. This is a single most important finding of our paper. It is also a practically important effect, as the internal alignment is perfect for grains at high attractor points and reduced for grains at lower attractor points. All in all, the present paper substantially extends our analysis in Paper I.

The limitations of the present study stem from the fact, that, while addressing the issue of how the degree of alignment changes in different circumstances, it does not calculate the degree of alignment exactly. This is done in Hoang & Lazarian (in preparation).

11.16 Towards modeling of grain alignment

Present day modeling of grain alignment both in molecular clouds (CL05; Pelkonen et al. 2007; Bethell et al. 2007) and accretion disks (Cho & Lazarian 2007) uses rather heuristic recipes for determining whether grains are aligned. In these studies the amplitude values of the RATs are calculated and used to calculate the maximal angular velocities achievable for a given damping of grain rotation. Such velocities parametrize the efficiencies of grain alignment in the chosen environments. In the paper above, we have confirmed the utility of such a parametrization and improved the criterion for the alignment to be efficient. However, we still have to obtain better measures of the expected alignment.

[12] An additional confusion in the aforementioned study stemmed from their claim that the prolate grains should align with long axes perpendicular to the alignment of the long axes of oblate grains. However, it was shown in Lazarian (1995) that both types of grains align the same way, if internal relaxation is accounted for.

12 SUMMARY

In the present paper, we studied the role of thermal fluctuations, thermal flipping, efficiency of H_2 torques and influence of random collisions on the RAT grain alignment for both the AMO and irregular grains. Our main results are summarized below:

1. We have used an AMO with inertia defined by a triaxial ellipsoid and averaged numerically RATs over thermal fluctuation. For this *ellipsoidal* AMO, we have found the increase of angular momentum of low-J attractor points from $J = 0$ to $J \sim J_{th}$. We also found the similar effect for irregular grains in which RATs are calculated using DDSCAT and for the entire spectrum of the ISRF.

2. We have proved that "wrong" alignment corresponding to low angular momentum for a narrow range of radiation direction reported in Paper I is eliminated when thermal fluctuations and thermal flipping are considered.

3. We have studied the crossover for the AMO and irregular grains and found that grains experience multiple crossovers before being trapped at low-J attractor points in the presence of thermal fluctuations.

4. We have found that random collisions of atomic gas increase the degree of alignment when grains are aligned by RATs with both low-J and high-J attractor points by driving grains from low-J to high-J attractor points. When the angular momentum of the high-J attractor point $J_{high}(\psi)$ greater than $3J_{th,gas}$, a significant degree of alignment can be achieved.

5. We have studied the influence of H_2 formation torques in the frame of the RAT alignment for different resurfacing times, showing that it can, in particular circumstances, enhance the degree of alignment with respect to the magnetic field.

ACKNOWLEDGMENTS

We thank Bruce Draine for clarifying to us some points in their DDSCAT code. TH acknowledges Joseph Weingartner for clarifications provided at the initial stage of this work. We thank Wayne Roberge and Ford for sharing with us their results from Roberge & Ford (2000). The support by the NSF Center for Magnetic Self-Organization in Laboratory and Astrophysical Plasmas and NSF grant AST 0507164 is acknowledged.

REFERENCES

Aiken D. K., Efstathiou A., McCall A., Hough J. H. 2002, MNRAS, 329, 647
Arce, H. G., Goodman, A. A., Bastien, P., Manset, N., Sumner, M. 1998, 499, 93
Andersson B-G, Potter S.B. 2007, ApJ, 665, 369
Bethell T., Cherpunov A., Lazarian A., Kim J. 2007, ApJ, 663, 1055
Cho J., Lazarian A. 2005, ApJ, 631, 361 (CL05)
Cho J.,& Lazarian A. 2007, ApJ, in press
Crutcher, R.M., Nutter, D.J., Ward-Thompson, D., & Kirk, J.M. 2004, ApJ, 600, 279
Davis L. Vistas in Astronomy, Volume 1, 1955, 336
Davis L., Greenstein J.L. 1951, ApJ, 114, 206
Dolginov A.Z. 1972, Ap&SS, 16, 337
Dolginov A.Z., Mytrophanov I.G. 1976, Ap&SS, 43, 291
Draine B., Flatau P. 1994, J. Opt. Soc. Am. A., 11, 1491
Draine B., Lee H. 1984, ApJ, 285, 89
Draine, B., Lazarian, A. 1999, ApJ, 512, 740
Draine B., Weingartner, J. 1996, ApJ, 470, 551 (DW96)
Draine B. Weingartner, J. 1997, ApJ, 480, 633 (DW97)
Gold T. 1952a, Nature, 169, 322
Gold T. 1952b, MNRAS, 112, 215
Goodman A., Jones T., Lada E., Myers P. 1995, ApJ, 448, 748
Greenberg, J.M 1968, in Nebulae and Interstellar Matter, eds, B.M Middlehurst & L.H. Aller (University of Chicago Press), 221-230
Hall J. 1949, Science, 109, 166
Harwit M. 1970, Nature, 226, 61
Hildebrand R., Davidson J. A., Dotson J.L, Wovell C.D., Novak G.,Vaillancourt J.E. 2000, PASP, 112, 1215
Hildebrand R. 2002, in *Astrophysical Spectropolarimetry*, ed. by J. Trujillo-Bueno, F. Moreno-Insertis, & F. Sanchez (Cambridge, UK: Cambridge Univ. Press), p. 265
Hiltner W. 1949, Science, 109, 165
Hough J.H., et al. 1989, MNRAS, 241, 71
Jones J.V., Spitzer L. 1967, ApJ, 146,943
Kim S.-H., Martin P. 1995, ApJ, 444, 293
Lai, S.-P., Crutcher, R.M., Girart, J.M., & Rao, R. 2002, ApJ, 566, 925
Landau L.D, & Lifshitz E. M. 1976, Mechanics (Oxford: Perganon)
Lazarian A. 1994, MNRAS, 268, 713
Lazarian A. 1995, ApJ, 453, 229
Lazarian A. 1997a, ApJ, 483, 296
Lazarian A. 1997b, MNRAS, 288, 609
Lazarian A., Efroimsky M. 1996, ApJ, 466, 274
Lazarian A., Efroimsky M., Ozik J. 1996, ApJ, 472, 240
Lazarian A., Efroimsky M. 1999, MNRAS, 303, 673
Lazarian A. 2003, J. Quant. Spectrosc. Rad. Trans., 79-80, 881
Lazarian A. 2007, J. Quant. Spectrosc. Rad. Trans., 106, 225
Lazarian A., Draine B. 1999a, ApJ, 516, L37
Lazarian A., Draine B. 1999b, ApJ, 520, L67
Lazarian A., Goodman A.A., Myers P.C. 1997, ApJ, 490, 273
Lazarian A., Roberge W. 1997, ApJ, 484, 230 (LR97)
Lazarian A., Hoang T. 2007a, MNRAS, 378, 910 (Paper I)
Lazarian A., Hoang T. 2007b, ApJL, 669, L77
Lazarian A., Yan H. 2002, ApJ, 566, L105-L108
Matthews B., Wilson C. 2000, ApJ, 531, 868
Matthews, B., Wilson, C.D., & Fiege, J.D. 2001, ApJ, 562, 400
Matthews B., Wilson C. 2002, ApJ, 574, 822
Mathis J. 1986, ApJ, 308, 281
Mathis J., Mezger P., Panagia N. 1983, A&A, 128, 212
Pagani L. et al. 2004, A&A, 413, 605
Pelkonen V. M, Juvela M., Padoan P. 2007, A&A, 461, 551
Purcell E. 1969, Physica, 41, 100
Purcell E. 1975, in Dusty Universe, eds. Field G.B., Cameron, A.G.W., New York: Neal Watson, 155
Purcell E. 1979, ApJ, 231, 404
Purcell E., Spitzer L. 1971, ApJ, 167, 31
Roberge W., Hanany S. 1990, B.A.A.S., 22, 862

Roberge W., DeGraff T.A., Flatherty J.E. 1993, ApJ, 418, 287
Roberge W., Hanany S., Messinger D. 1995, 453, 238
Roberge W.G., & Lazarian, A. 1999, MNRAS, 305, 615
Serkowski K. 1973, in IAU Symp. 52, Interstellar Dust and Related Topics, eds. J.M. Greenberg & H. C. van de Hulst (Dordrecht:Reidel), 145
Spitzer L., McGlynn T. 1979, ApJ, 231, 417
Spitzer L, Tukey, 1951, ApJ, 114, 187
Ward-Thompson D., Kirk J.M, Crutcher et al. 2000, ApJ, 537, L135
Ward-Thompson D., Andre P., Kirk, J. 2002, MNRAS, 329, 257
Weingartner J., & Draine B. 2003, ApJ, 589, 289 (WD03)
Whittet D.C.B., Gerakines P.A., J.H. Hough Shenoy 2001, ApJ, 547, 872
Whittet D.C.B, Hough J.H, Lazarian A., Hoang T. 2007, ApJ, submitted
Yan H., & Lazarian A. 2003, ApJ, 592, L33-36
Yan H., Lazarian A., Draine B. 2004, ApJ, 616, 895

APPENDIX A: RELATION OF ANGLES Θ, β, Φ AND ξ, ϕ, ψ

$$\cos\Theta = \hat{\mathbf{a}}_1.\hat{\mathbf{e}}_1, \tag{A1}$$

$$\Phi = 2tan^{-1}\left(\frac{\sin\Theta - \hat{\mathbf{a}}_1.\hat{\mathbf{e}}_2}{\hat{\mathbf{a}}_1.\hat{\mathbf{e}}_3}\right), \tag{A2}$$

$$\beta = 2tan^{-1}\left(\frac{\sin\Theta + \hat{\mathbf{a}}_2.\hat{\mathbf{e}}_2}{\sin\Theta(\hat{\mathbf{a}}_2.\hat{\mathbf{e}}_3\cos\Phi - \hat{\mathbf{a}}_2.\hat{\mathbf{e}}_2\sin\Phi)}\right), \tag{A3}$$

where $\hat{\mathbf{a}}_1, \hat{\mathbf{a}}_2, \hat{\mathbf{a}}_3$ are unit vectors in grain reference, and $\hat{\mathbf{e}}_1, \hat{\mathbf{e}}_2, \hat{\mathbf{e}}_3$ are unit vectors in the lab system. Dot products in above equations can be obtained from following expressions

$$\hat{\mathbf{a}}_i.\hat{\mathbf{e}}_1 = \cos\psi\hat{\mathbf{z}}_B.\hat{\mathbf{a}}_i - \sin\psi\hat{\mathbf{x}}_B.\hat{\mathbf{a}}_i, \tag{A4}$$

$$\hat{\mathbf{a}}_i.\hat{\mathbf{e}}_2 = \cos\psi\hat{\mathbf{x}}_B.\hat{\mathbf{a}}_i - \sin\psi\hat{\mathbf{z}}_B.\hat{\mathbf{a}}_i, \tag{A5}$$

$$\hat{\mathbf{a}}_i.\hat{\mathbf{e}}_3 = \hat{\mathbf{y}}_B.\hat{\mathbf{a}}_i, \tag{A6}$$

where

$$\begin{aligned}\hat{\mathbf{x}}_B.\hat{\mathbf{a}}_1 =& \hat{\mathbf{x}}\xi\cos\phi\sin\zeta\sin\gamma + \sin\phi\cos\zeta\sin\gamma \\ &+ \sin\xi\cos\phi\cos\gamma,\end{aligned} \tag{A7}$$

$$\hat{\mathbf{z}}_B.\hat{\mathbf{a}}_1 = \cos\xi\cos\gamma - \sin\xi\sin\zeta\sin\gamma, \tag{A8}$$

$$\begin{aligned}\hat{\mathbf{y}}_B.\hat{\mathbf{a}}_1 =& \cos\xi\sin\phi\sin\zeta\sin\gamma - \cos\phi\cos\zeta\sin\gamma \\ &+ \sin\xi\sin\phi\cos\gamma,\end{aligned} \tag{A9}$$

$$\begin{aligned}\hat{\mathbf{x}}_B.\hat{\mathbf{a}}_2 =& \cos\xi\cos\phi(\cos\alpha\cos\zeta - \sin\alpha\sin\zeta\cos\gamma) \\ &- \sin\phi(\cos\alpha\sin\zeta + \sin\alpha\cos\zeta\cos\gamma) \\ &+ \sin\xi\cos\phi\sin\alpha\sin\gamma,\end{aligned} \tag{A10}$$

$$\begin{aligned}\hat{\mathbf{z}}_B.\hat{\mathbf{a}}_2 =& -\sin\xi(\cos\alpha\cos\zeta - \sin\alpha\sin\zeta\cos\gamma) \\ &+ \cos\xi\sin\alpha\sin\gamma,\end{aligned} \tag{A11}$$

$$\begin{aligned}\hat{\mathbf{y}}_B.\hat{\mathbf{a}}_2 =& \cos\xi\sin\phi(\cos\alpha\cos\zeta - \sin\alpha\sin\zeta\cos\gamma) \\ &+ \cos\phi(\cos\alpha\sin\zeta + \sin\alpha\cos\zeta\cos\gamma) \\ &+ \sin\xi\sin\phi\sin\alpha\sin\gamma,\end{aligned} \tag{A12}$$

$$\tag{A13}$$

with $\hat{\mathbf{x}}_B, \hat{\mathbf{y}}_B, \hat{\mathbf{z}}_B$ are unit vectors of magnetic field coordinate system in which $\hat{\mathbf{z}}_B \| \mathbf{B}$. Here α, γ, ζ are Euler angles shown in Fig. A1.

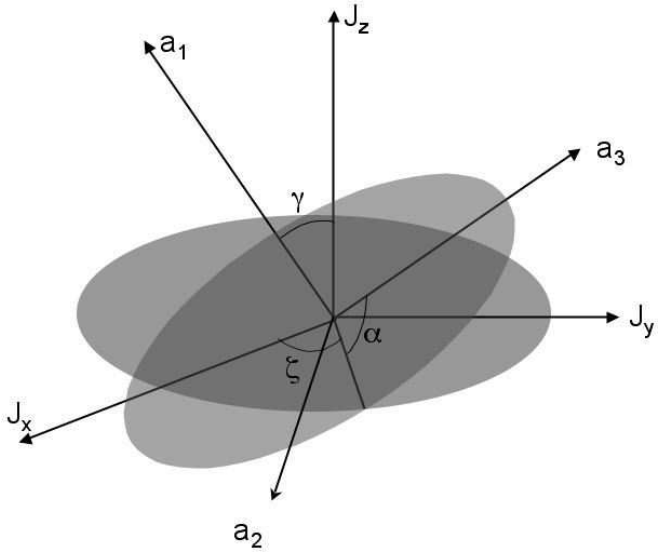


Figure A1. Orientation of principal axes in the angular coordinate system are described by Euler angles γ, α and ζ.

APPENDIX B: RATS

Similar to Paper I, in order to make an easy relation of our results to those in earlier works, wherever it is possible, we preserve notations adopted in DW97. Mean radiative torque efficiency over wavelengths, $\overline{\mathbf{Q}(\Theta,\beta,\Phi)}$ is defined as

$$\overline{\mathbf{Q}} = \frac{\int \mathbf{Q}_\lambda u_\lambda d\lambda}{\int u_\lambda d\lambda}, \tag{B1}$$

where u_λ is the energy density (see Mathis, Mezger & Panagia 1983), and $\mathbf{Q}_\lambda$ is the RAT efficiency corresponding to wavelength λ. RAT from the anisotropic component of radiation is defined by

$$\mathbf{\Gamma}_{rad} = \frac{\overline{u}_{rad} a_{eff}^2 \overline{\lambda}}{2}\gamma\overline{\mathbf{Q}}. \tag{B2}$$

where γ is the anisotropy degree of radiation, a_{eff} is the effective size of the grain (see DW96; Paper I), $\overline{\lambda}, \overline{u}_{rad}$ are mean wavelength and mean energy density of radiation field, which are respectively given by

$$\overline{\lambda} = \frac{\int \lambda d\lambda}{\int d\lambda}, \tag{B3}$$

$$\overline{u}_{rad} = \frac{\int u_\lambda \lambda d\lambda}{\int \lambda d\lambda}. \tag{B4}$$

APPENDIX C: AVERAGING OVER FREE-TORQUE MOTION

Consider an ellipsoid with three principal axes $\mathbf{a}_1, \mathbf{a}_2, \mathbf{a}_3$ and moment of inertia $I_1 > I_2 > I_3$, respectively. Dynamics of such an ellipsoid is clearly presented in the textbook of Landau & Liftshift (1972). Let define a dimensionless quantity

$$k^2 = \frac{(I_2 - I_3)(q-1)}{(I_1 - I_2)(1 - I_3 q/I_1)}, \tag{C1}$$

where $q = \frac{2I_1 E}{J^2}$ is the ratio of total kinetic energy to the rotational energy along the maximal inertia axis.

For $q < I_1/I_2, k^2 < 1$, the solution of Euler equations is

$$\omega_1 = \pm\frac{J}{I_1}(\frac{I_1 - I_3 q}{I_1 - I_3})^{1/2} dn(\tau), \tag{C2}$$

$$\omega_2 = -\frac{J}{I_2}(\frac{I_2(q-1)}{I_1 - I_2})^{1/2} sn(\tau), \tag{C3}$$

$$\omega_3 = \pm\frac{J}{I_3}(\frac{I_3(q-1)}{I_1 - I_3})^{1/2} cn(\tau) \tag{C4}$$

where cn, sn, tan are hyperbolic trigonometric functions, and τ is given by

$$\tau \equiv tJ\left[\frac{(I_1 - I_2)(1 - I_3 q/I_1)}{I_1 I_2 I_3}\right]^{1/2}. \tag{C5}$$

The rotation period around the maximal inertia axis is

$$P_\tau = 4F(\pi/2, k^2), \tag{C6}$$

where F is the elliptic integral defined by

$$F(\epsilon, m) = \int_0^\epsilon d\theta (1 - m\sin^2\theta)^{-1/2}. \tag{C7}$$

For $q > I_1/I_2$, angular velocities are given by

$$\omega_1 = \pm\frac{J}{I_1}(\frac{I_1 - I_3 q}{I_1 - I_3})^{1/2} cn(\tau), \tag{C8}$$

$$\omega_2 = -\frac{J}{I_2}(\frac{I_2(1 - I_3 q)}{I_2 - I_3})^{1/2} sn(\tau), \tag{C9}$$

$$\omega_3 = \pm\frac{J}{I_3}(\frac{I_3(q-1)}{I_1 - I_3})^{1/2} dn(\tau), \tag{C10}$$

where

$$\tau \equiv tJ\left[\frac{(I_2 - I_3)(q-1)}{I_1 I_2 I_3}\right]^{1/2}. \tag{C11}$$

Rotation period for this case is given by

$$P_\tau = 4F(\pi/2, k^2). \tag{C12}$$

In above equations, $\pm$ stand for the positive and negative flipping states.

Euler angles α, γ, ζ (see Fig. A1) can be deduced from angular velocity as followings

$$\sin\,\alpha\,\sin\,\gamma = \frac{I_2\omega_2}{J}, \tag{C13}$$

$$\cos\,\alpha\,\sin\,\gamma = \frac{I_3\omega_3}{J}, \tag{C14}$$

$$\cos\,\gamma = \frac{I_1\omega_1}{J}. \tag{C15}$$

WD04 averaged RATs over free torque motion as following,

$$\overline{A}(q) = \frac{1}{P_\tau}\int_0^{P_\tau} d\tau \frac{1}{2\pi}\int_0^{2\pi} A(\alpha, \zeta, \gamma). \tag{C16}$$

Here they assume that the rotation of the grain about the angular momentum is much faster than the rotation about the maximal inertia axis (i.e. at each a moment t with angles γ and α, the angle ζ can vary from 0 to 2π). Clearly, this assumption is not correct because these processes are comparable. We have implemented an algorithm to average RATs over free torque motion in which the angle ζ is obtained by solving an Euler differential equation. We found that RATs obtained by our method are in good agreement with what obtained using equation (C16) when they are averaged over a time scale greater than $10^3 P_\tau$.

APPENDIX D: AVERAGING OVER THERMAL FLUCTUATIONS

Average of a quantity A over thermal fluctuations is defined by

$$\langle A\rangle = \frac{\int_0^1 ds A(q,J)\exp[-q(s)J^2/2I_1 kT_d]}{\int ds \exp[-qJ^2/2I_1 kT_d]}. \tag{D1}$$

Number of state s in equation (D1) is given by

$$s \equiv 1 - \frac{2}{\pi}\int_0^{\alpha_1} d\alpha \left[\frac{I_3(I_1 - I_2 q) + I_1(I_2 - I_3)\cos^2\alpha}{I_3(I_1 - I_2) + I_1(I_2 - I_3)\cos^2\alpha}\right]^{1/2}, \tag{D2}$$

with α_1 is given by

$$\alpha_1 = \cos^{-1}\left[\frac{I_3(I_2 q - I_1)}{I_1(I_2 - I_3)}\right]^{1/2}, \tag{D3}$$

for $q > I_1/I_2$, and $\alpha_1 = \pi/2$ for $q \leqslant I_1/I_2$ (see WD03).